Thirty years of GO-SHIP and WOCE data: Atlantic overturning of mass, heat, freshwater, and anthropogenic Carbon transport

Verónica Caínzos

In collaboration with:

Instituto de Oceanografía y Cambio Global (IOCAG – ULPGC): Alonso Hernández-Guerra, M. Dolores Pérez-Hernández, and others

Instituto de Investigaciones Marinas (IIM – CSIC): Fiz F. Pérez, Antón Velo

NORCE Norwegian Research Centre & National Oceanography Centre (NOC): Elaine McDonagh

ICARUS – Maynooth University: Gerard McCarthy

7th Summer School on Theory, Mechanisms and Hierarchical Modelling of Climate Dynamics
Estimating Ocean Transports: Single Sections, Box Models and Reanalysis Products
ICTP Trieste, Italy | 29 June - 11 July, 2026

Outline

- **Introduction**
- AMOC: overturning of mass, heat, freshwater
- Atlantic budget of Anthropogenic Carbon (C_{anth})

The Atlantic Meridional Overturning Circulation

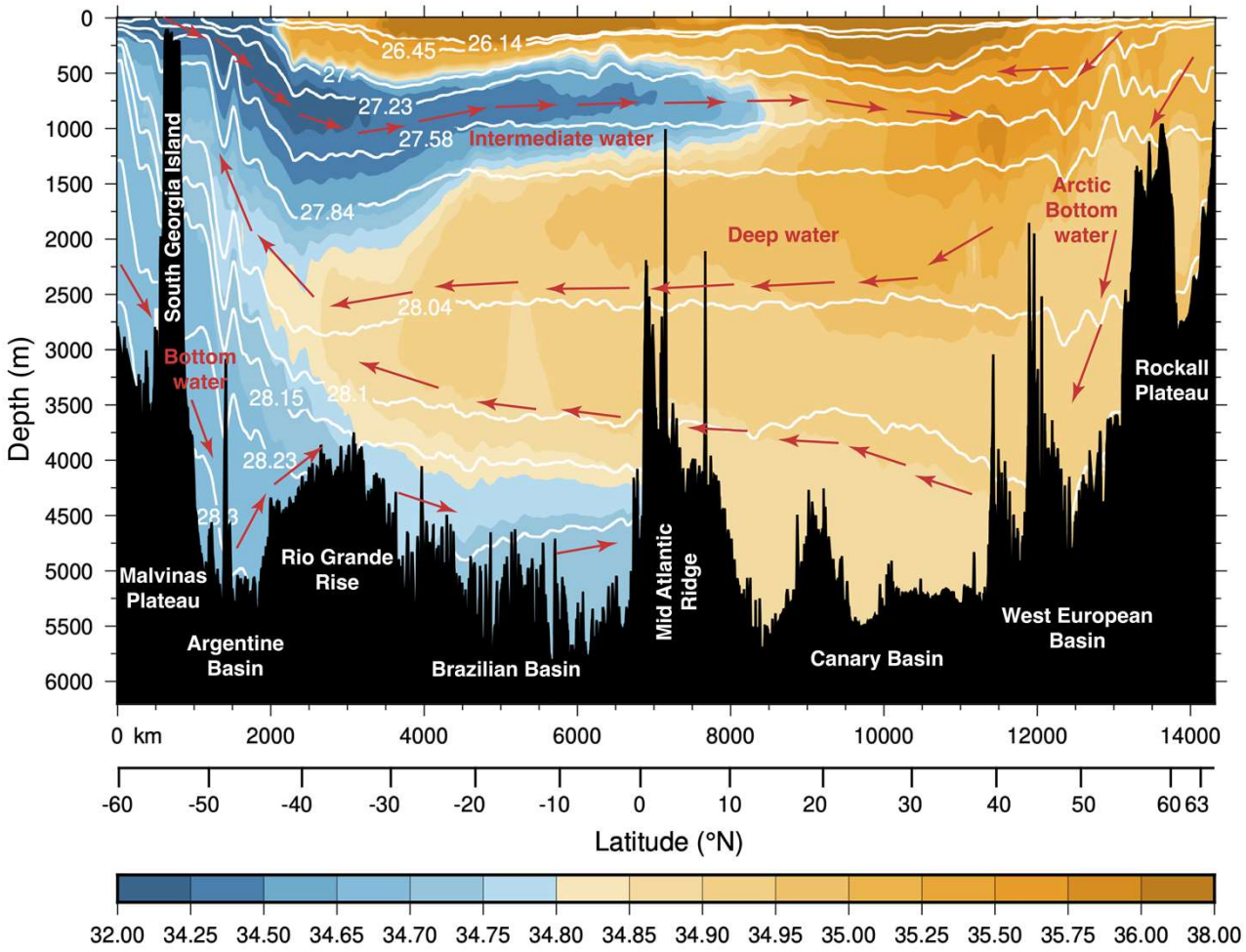

The Atlantic Meridional Overturning Circulation

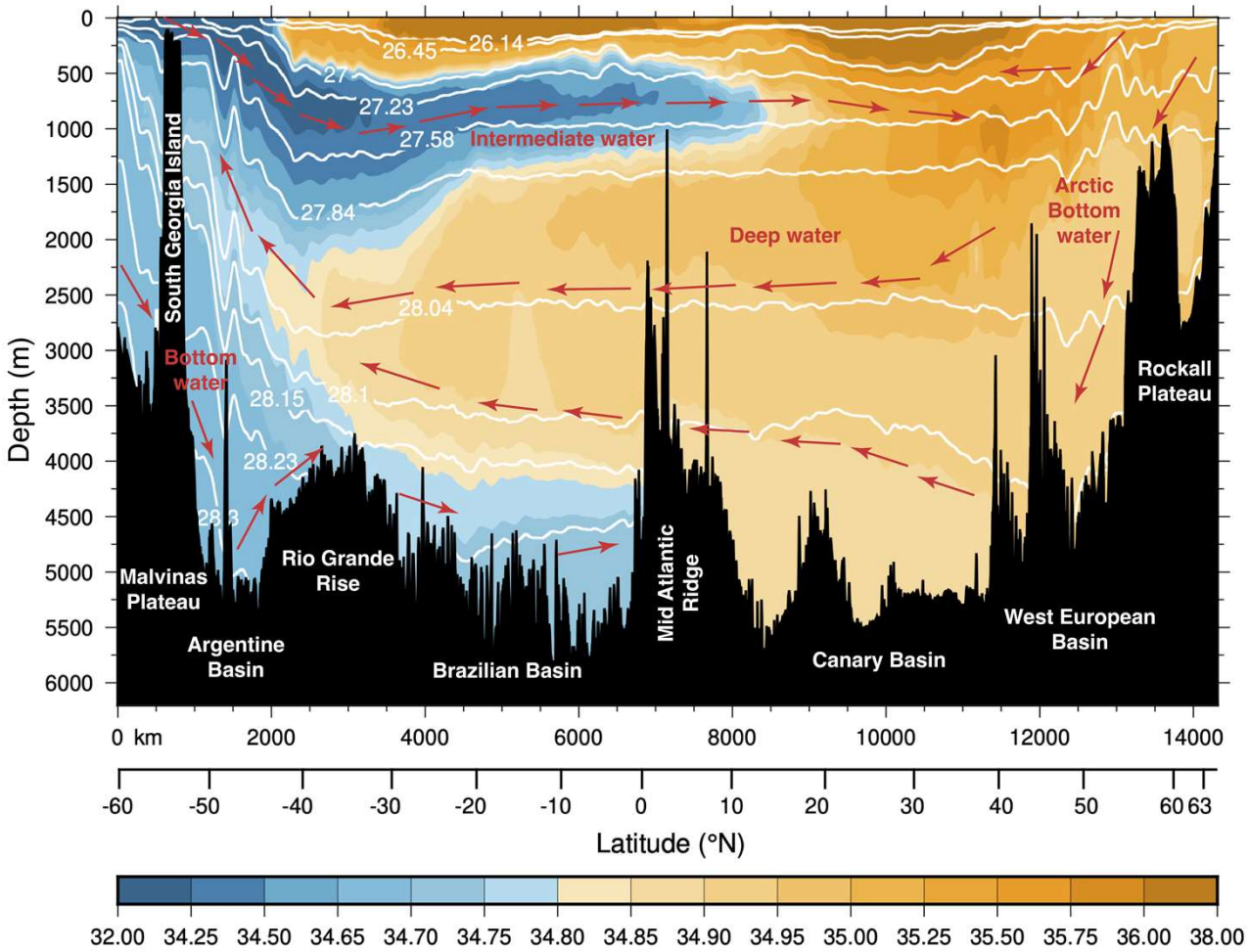

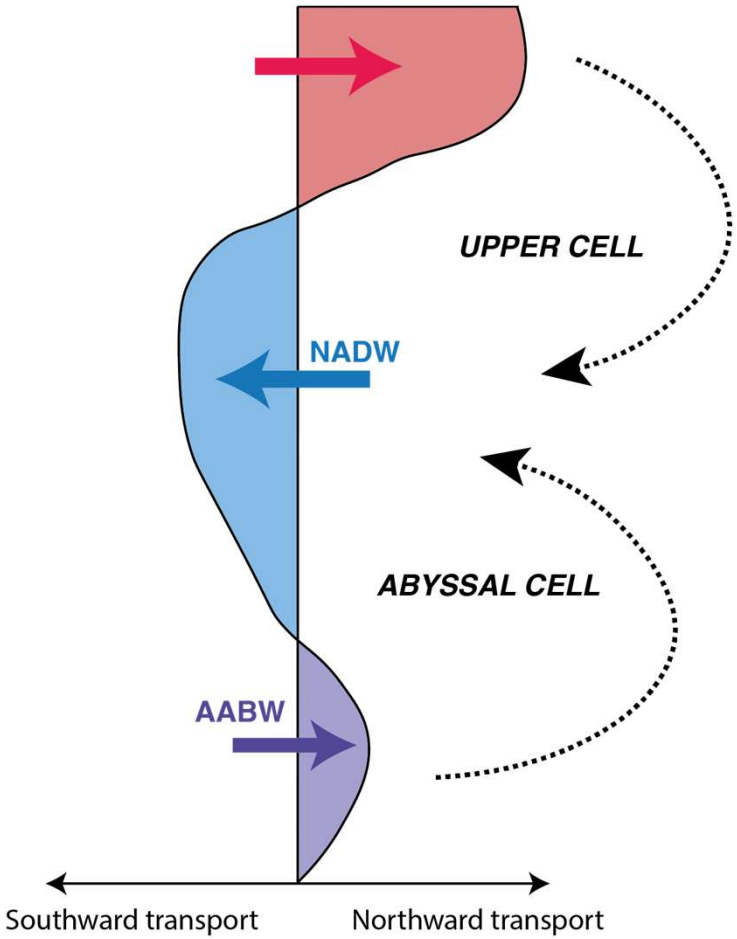

Adapted from Kersalé et al., 2020

Timescales of AMOC variability

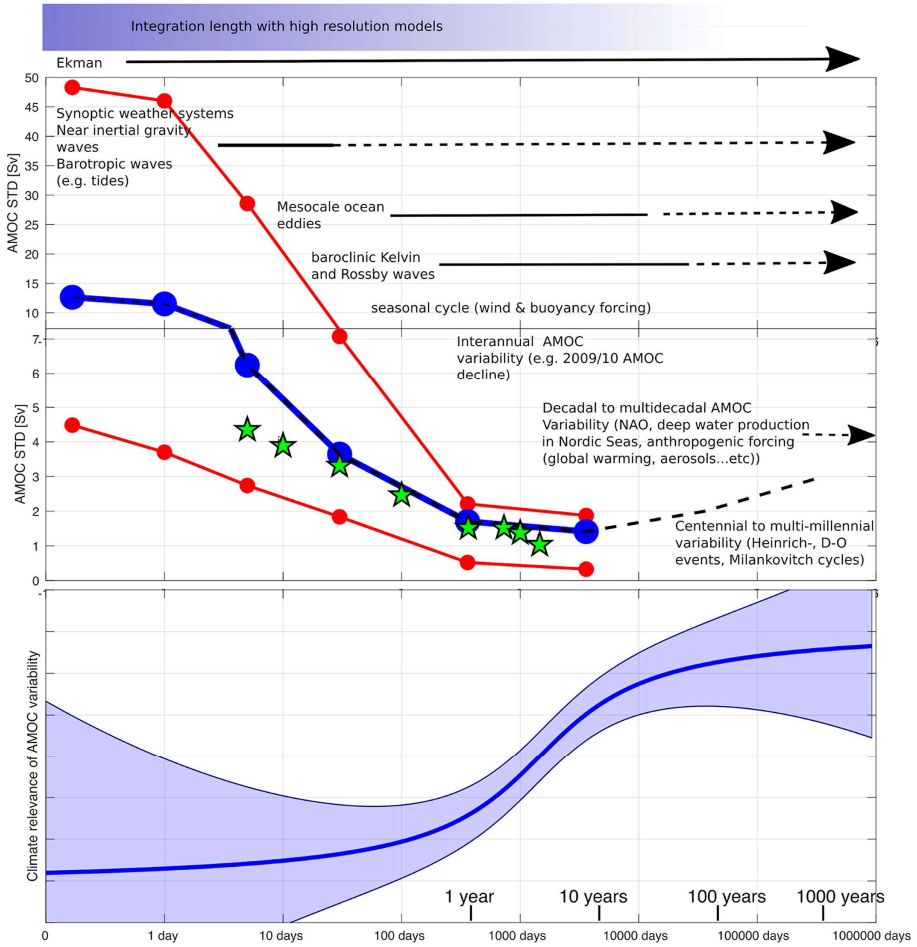

Hirschi et al. 2020

Region-dependent

Subtropics: - wind forcing at higher frequencies

- buoyancy forcing at lower frequencies

SPNA: - buoyancy and wind forcing at low frequencies (linked to NAO)

MOC quantified with hydrographic data

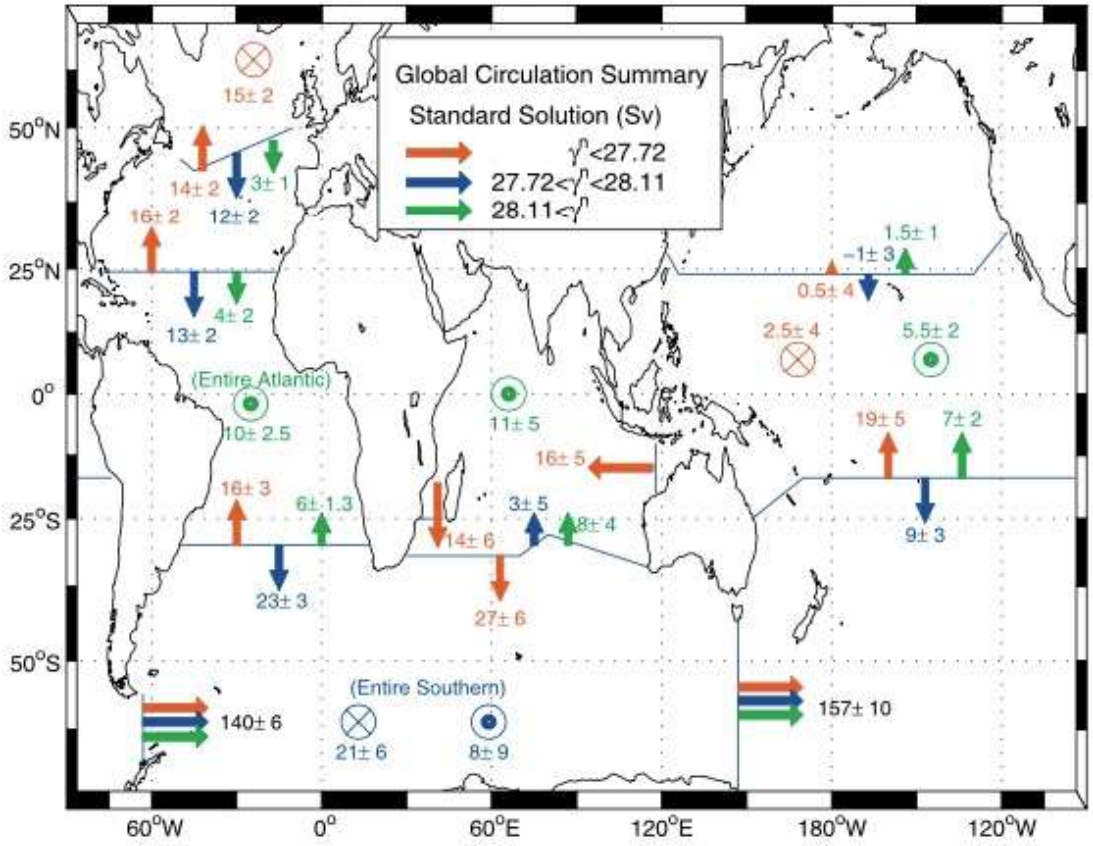

Ganachaud, 2003

World Ocean Circulation Experiment (WOCE) program

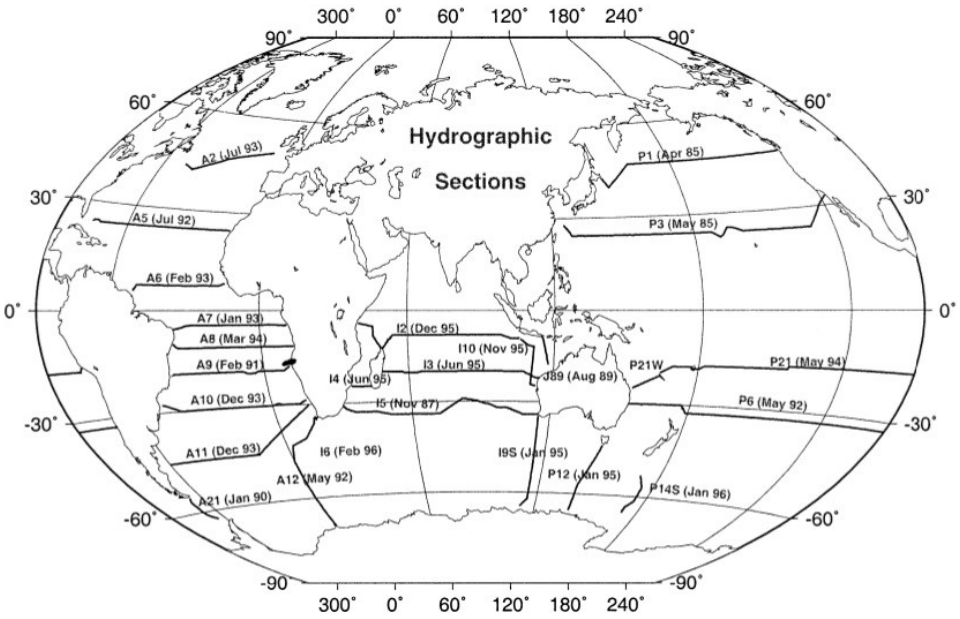

Ganachaud & Wunsch, 2003

AMOC reconstruction with proxies

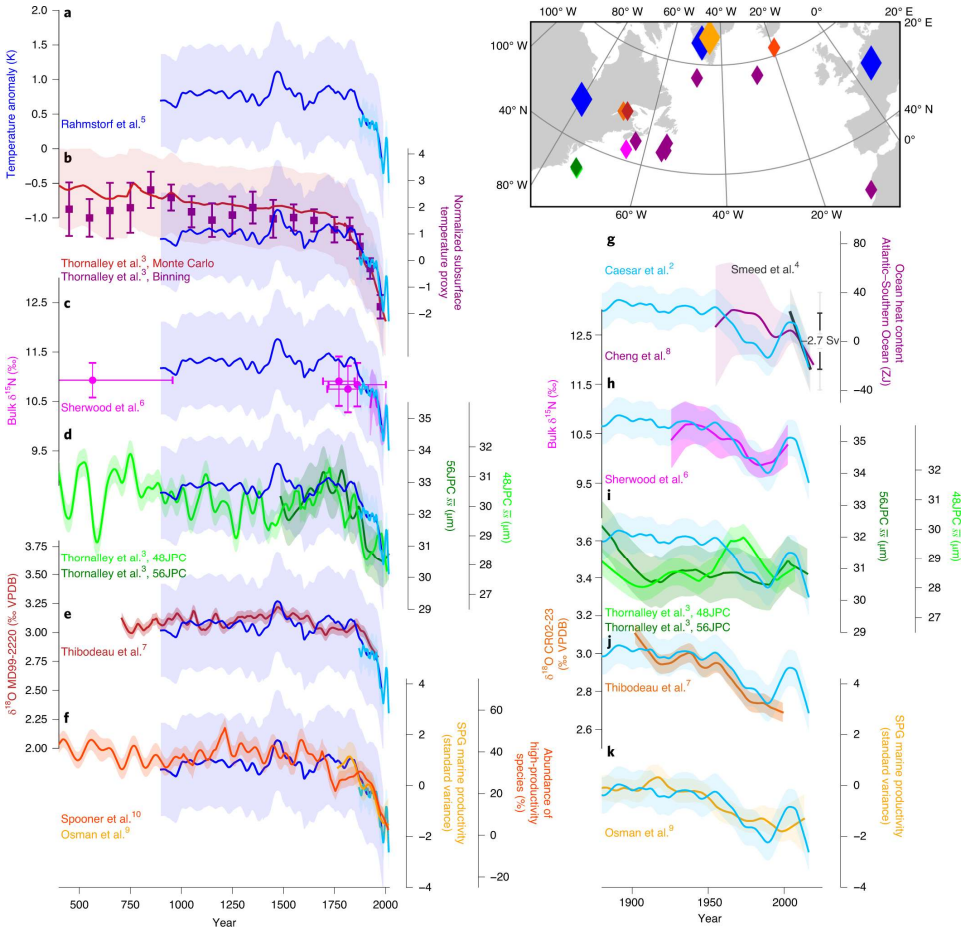

Caesar et al. 2021

AMOC reconstruction with proxies

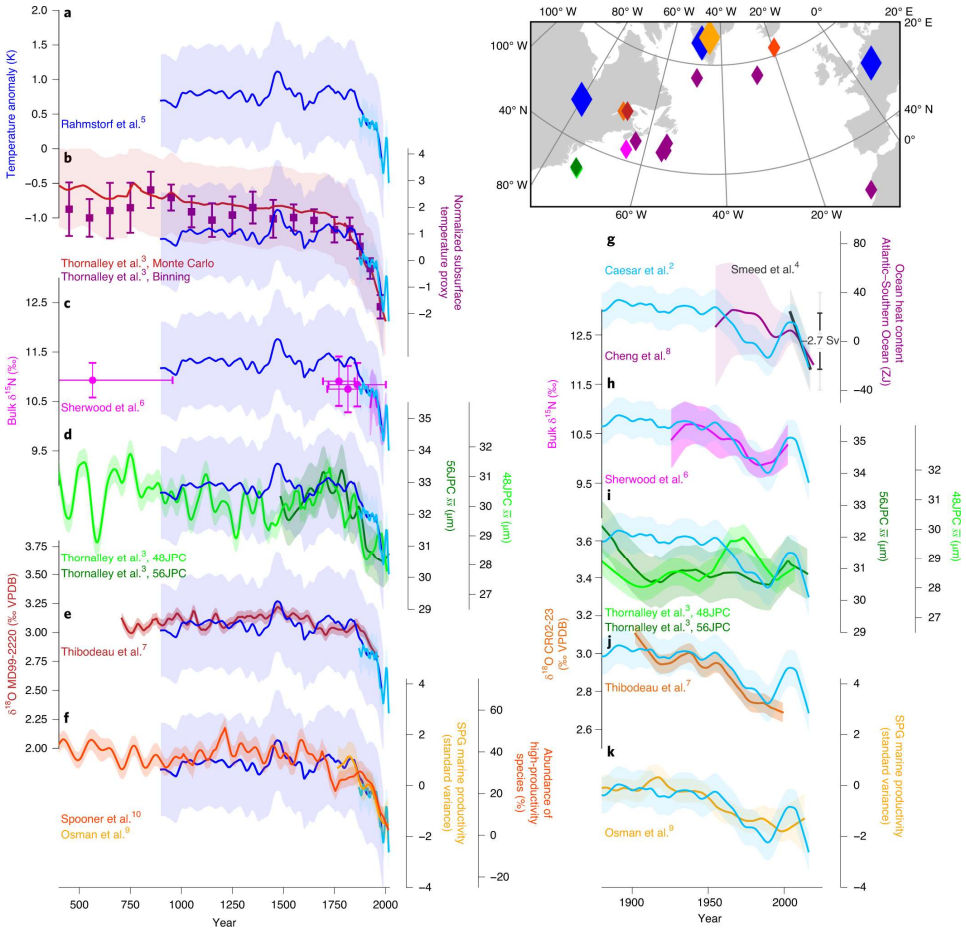

Caesar et al. 2021

AMOC projections with models

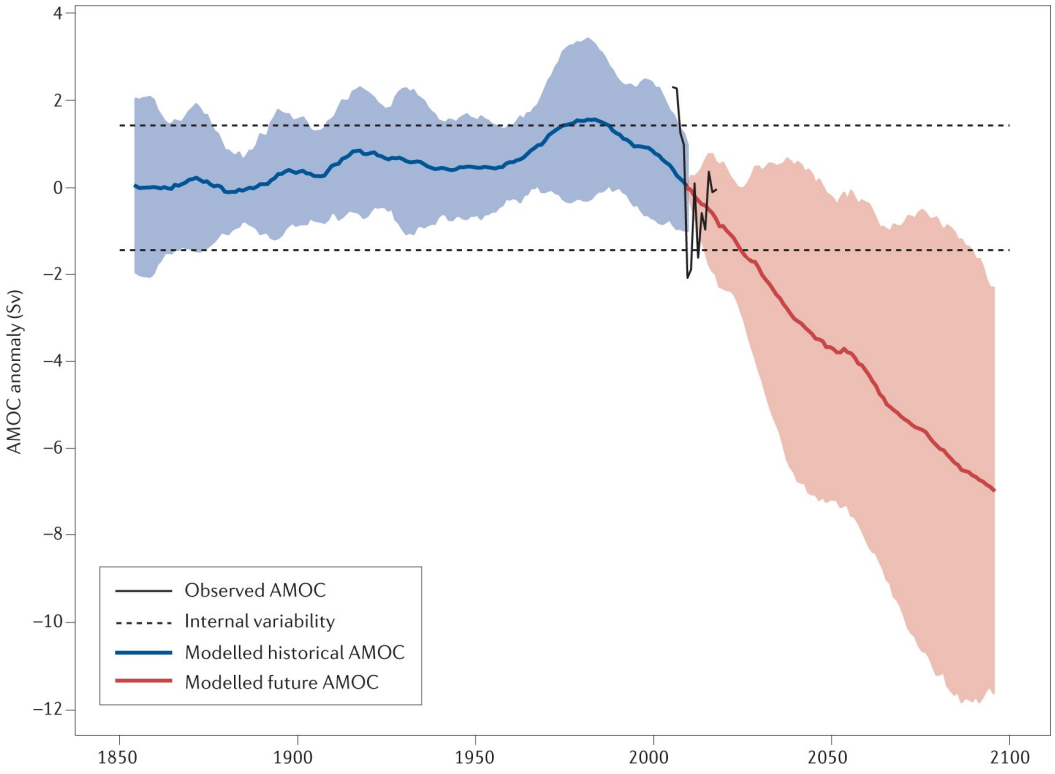

Jackson et al. 2022

Outline

- Introduction
- **AMOC: overturning of mass, heat, freshwater**

  Caínzos et al., 2022 *(GRL)*
- Atlantic budget of Anthropogenic Carbon (C_{anth})

AMOC monitoring

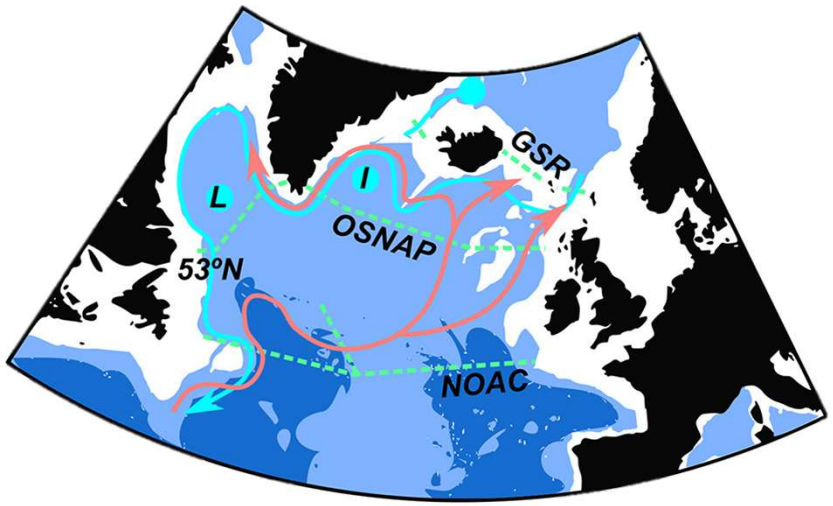

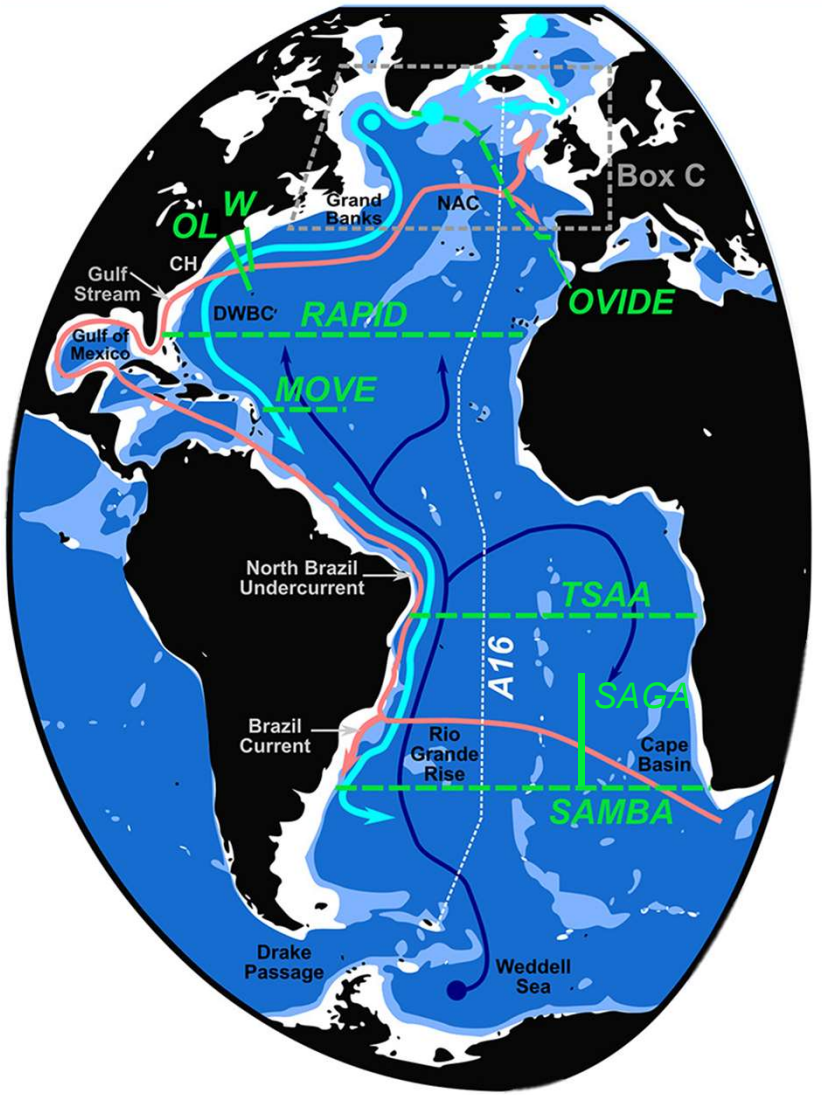

McCarthy et al., 2020

Three inversions for the last three decades: WOCE & GO-SHIP data

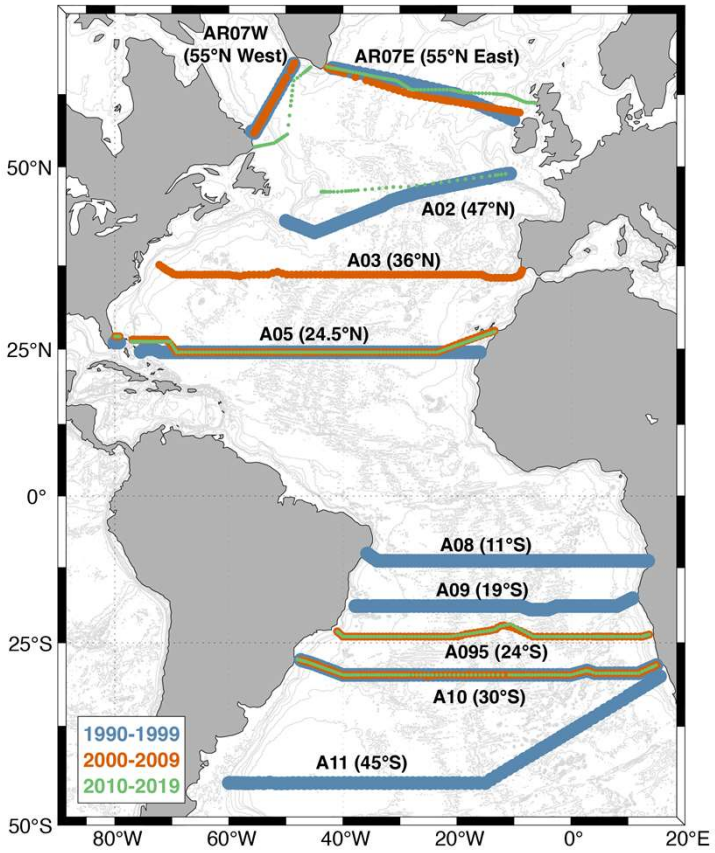

Three inversions for the last three decades: WOCE & GO-SHIP data

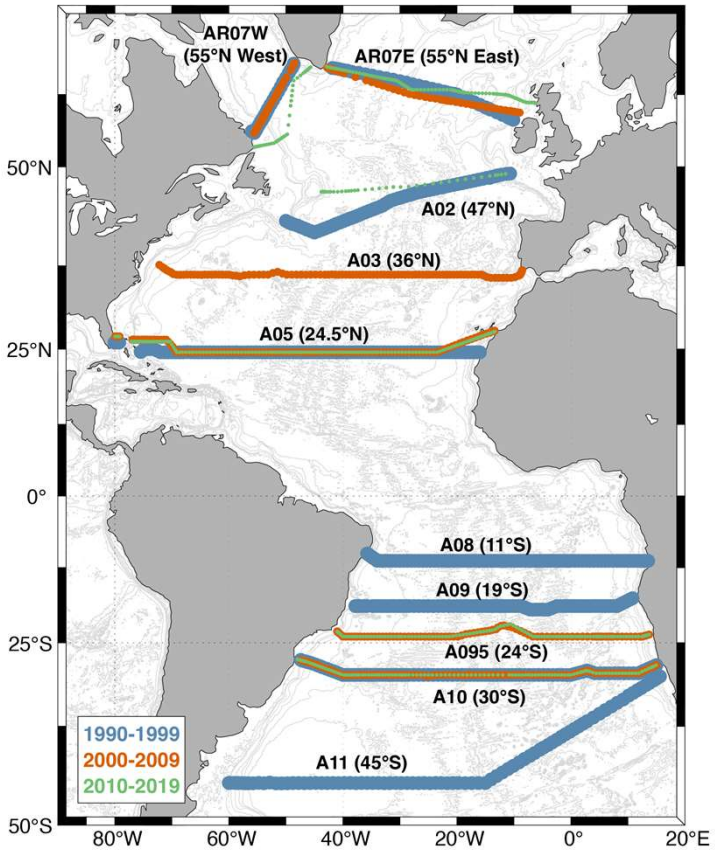

Vertical sections A10 – 30ºS

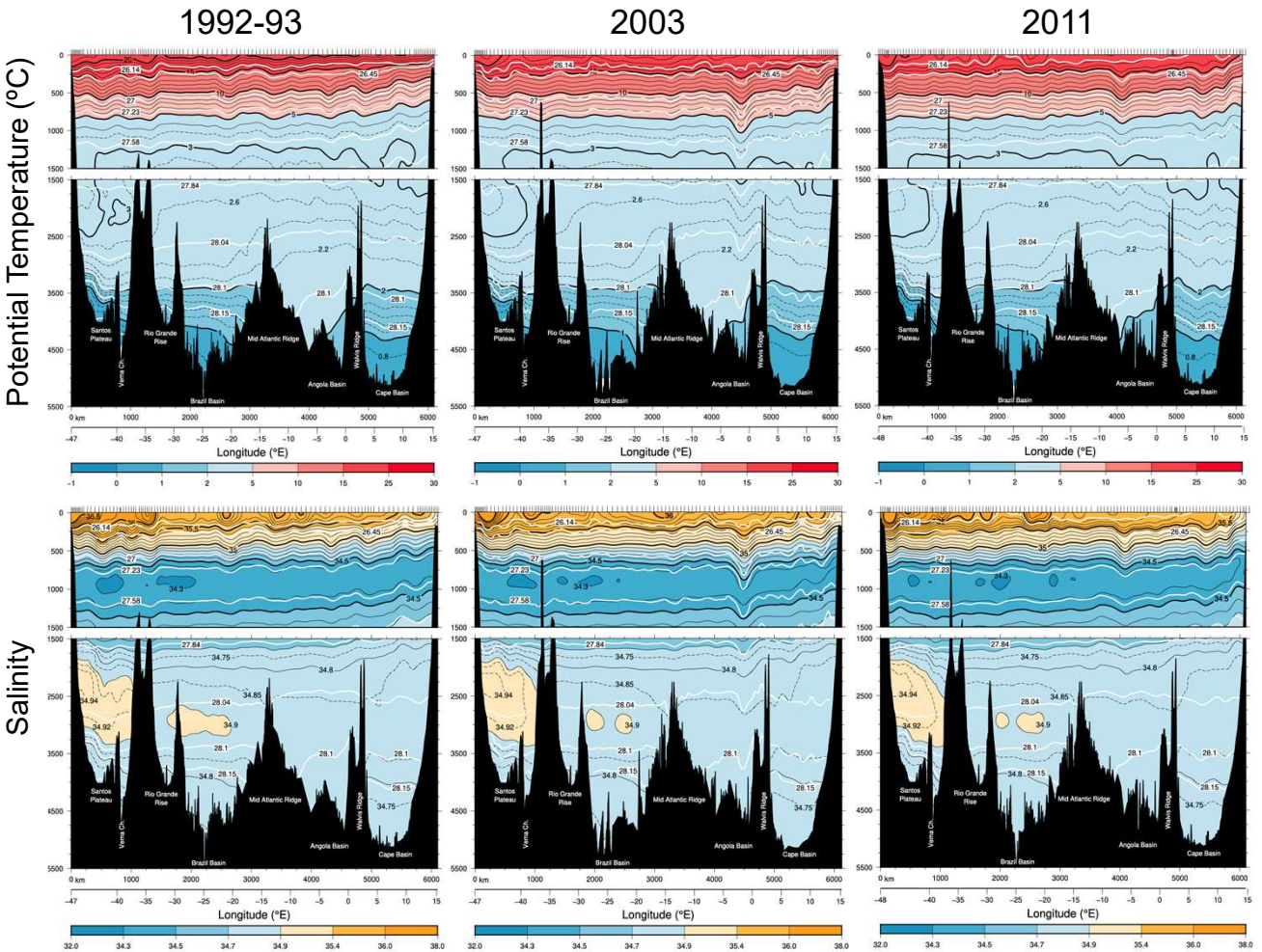

Inverse modelling - MASS + SALT

Total conservation for each box (both sections)

Regional constraints for each section

Conservation for each layer (both sections)

Total conservation for each section

$$
\begin{pmatrix}
e_{A_{t,1}} & \cdots & e_{A_{t,n}} & e_{B_{t,1}} & \cdots & e_{B_{t,m}} & 1 & 1 \\
e_{A_{reg}} & \cdots & e_{A_{reg}} & 0 & \cdots & 0 & 0 & 0 \\
0 & \cdots & 0 & e_{B_{reg}} & \cdots & e_{B_{reg}} & 0 & 0 \\
e_{A_{1,1}} & \cdots & e_{A_{1,n}} & e_{B_{1,1}} & \cdots & e_{B_{1,n}} & 1 & 1 \\
e_{A_{2,1}} & \cdots & e_{A_{2,n}} & e_{B_{2,1}} & \cdots & e_{B_{2,n}} & 0 & 0 \\
\vdots & \ddots & \vdots & \vdots & \ddots & \vdots & 0 & 0 \\
\vdots & \ddots & \vdots & \vdots & \ddots & \vdots & \vdots & \vdots \\
e_{A_{q-1,1}} & \cdots & e_{A_{q-1,n}} & e_{B_{q-1,1}} & \cdots & e_{B_{q-1,n}} & 0 & 0 \\
e_{A_{q,1}} & \cdots & e_{A_{q,n}} & e_{B_{q,1}} & \cdots & e_{B_{q,n}} & 0 & 0 \\
s_{A_{t,1}} & \cdots & s_{A_{t,n}} & 0 & \cdots & 0 & \overline{\left(\frac{s_{A_1}}{e_{A_1}}\right)} & 0 \\
0 & \cdots & 0 & s_{B_{t,1}} & \cdots & s_{B_{t,m}} & 0 & \overline{\left(\frac{s_{B_1}}{e_{B_1}}\right)}
\end{pmatrix}
\begin{pmatrix}
b_{A_1} \\ \vdots \\ b_{A_n} \\ b_{B_1} \\ \vdots \\ b_{B_m} \\ \Delta T_{A_{Ek}} \\ \Delta T_{B_{Ek}}
\end{pmatrix}
=
\begin{pmatrix}
y_{A_t} + y_{B_t} + T_{A_{Ek}} + T_{B_{Ek}} \\
y_{A_{reg}} \\
y_{B_{reg}} \\
y_{A_1} + y_{B_1} + T_{A_{Ek}} + T_{B_{Ek}} \\
y_{A_2} + y_{B_2} \\
\vdots \\
\vdots \\
y_{A_{q-1}} + y_{B_{q-1}} \\
y_{A_q} + y_{B_q} \\
z_t + T_{A_{Ek}} \cdot \overline{\left(\frac{s_{A_1}}{e_{A_1}}\right)} \\
z_{B_t} + T_{B_{Ek}} \cdot \overline{\left(\frac{s_{B_1}}{e_{B_1}}\right)}
\end{pmatrix}
$$

e: mass *y: mass transport*
s: salt *z: salt transport*

b: reference velocities
ΔT_{Ek}: Ekman correction
T_{Ek}: Ekman transport

n: number of pair of stations for section A
m: number of pair of stations for section B
q: number of layers (11)

Two counter-rotating overturning cells

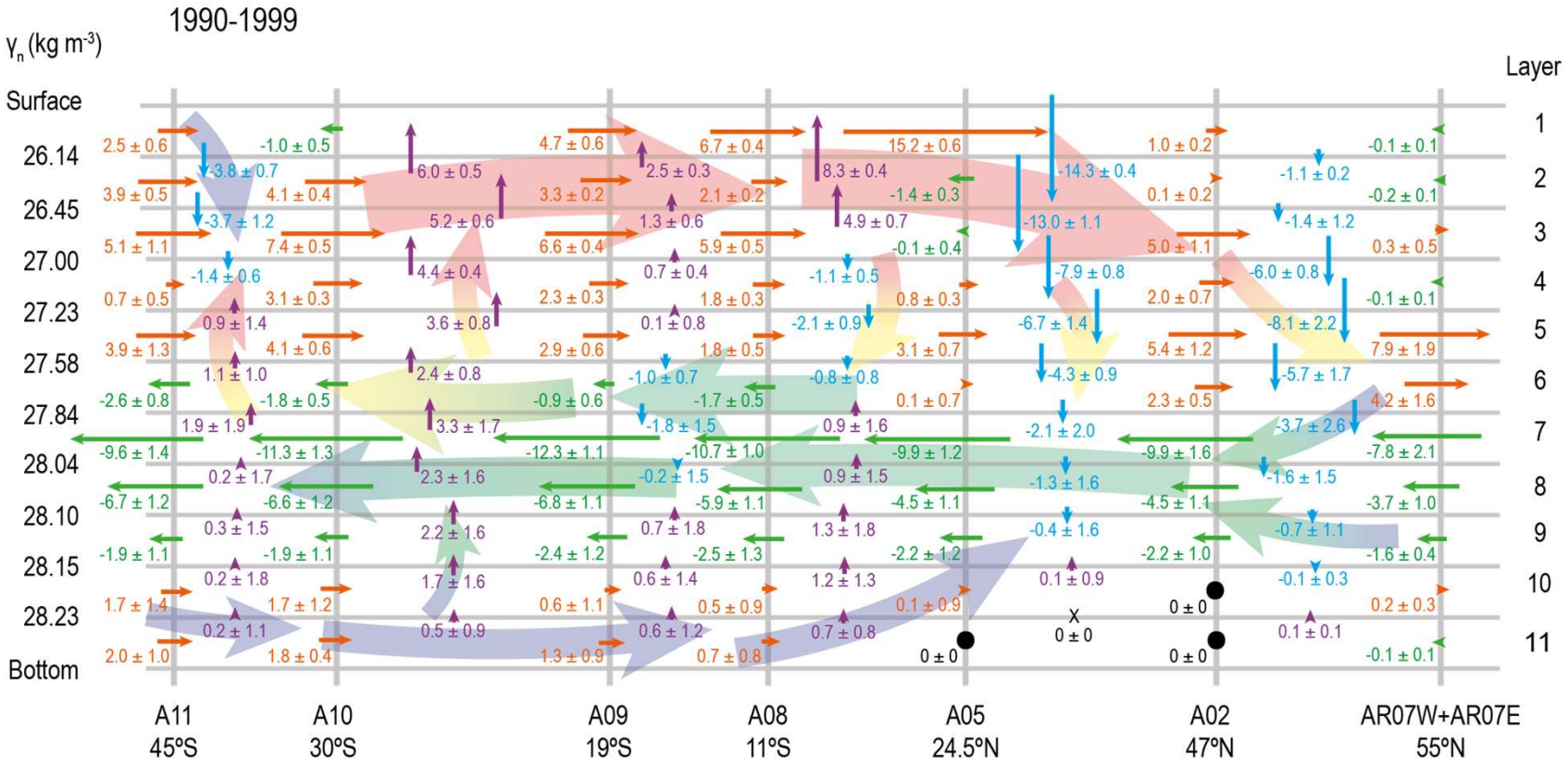

Two counter-rotating overturning cells

Upwelling in South Atlantic subtropical gyre

Downwelling in North Atlantic subtropical gyre and SPNA

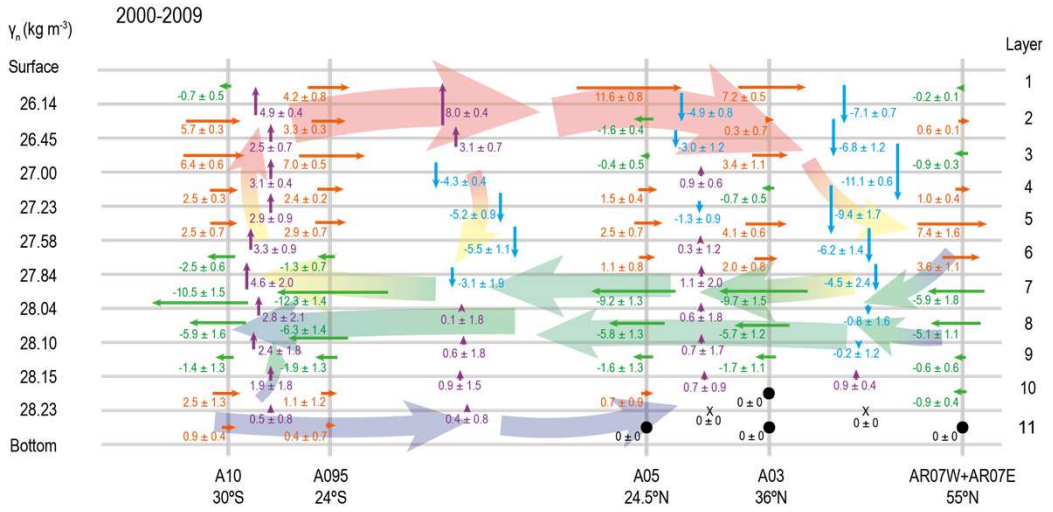

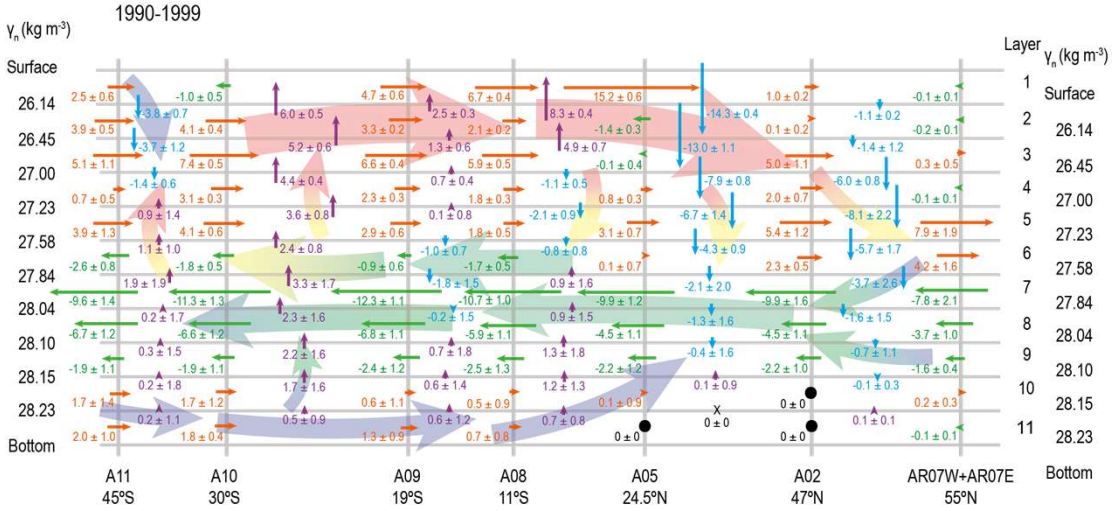

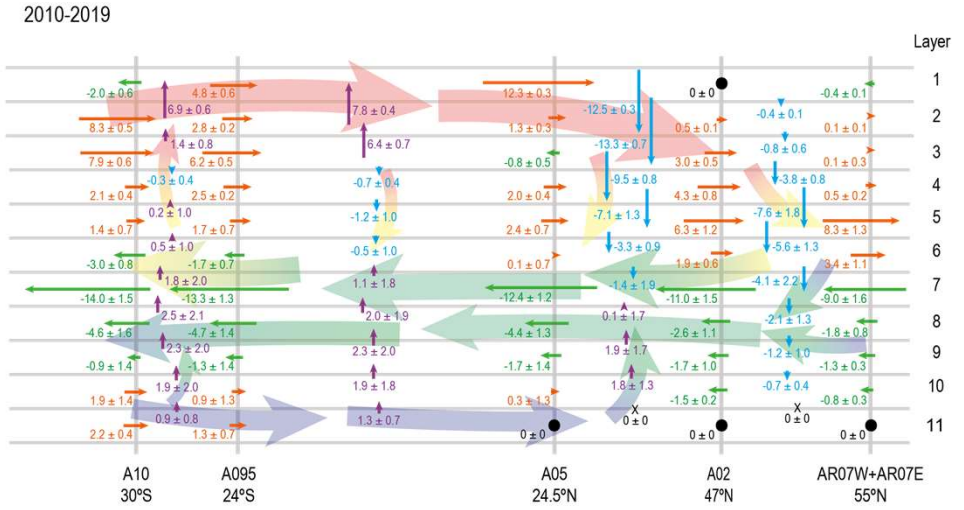

No significant trends for AMOC at any latitude for the last three decades

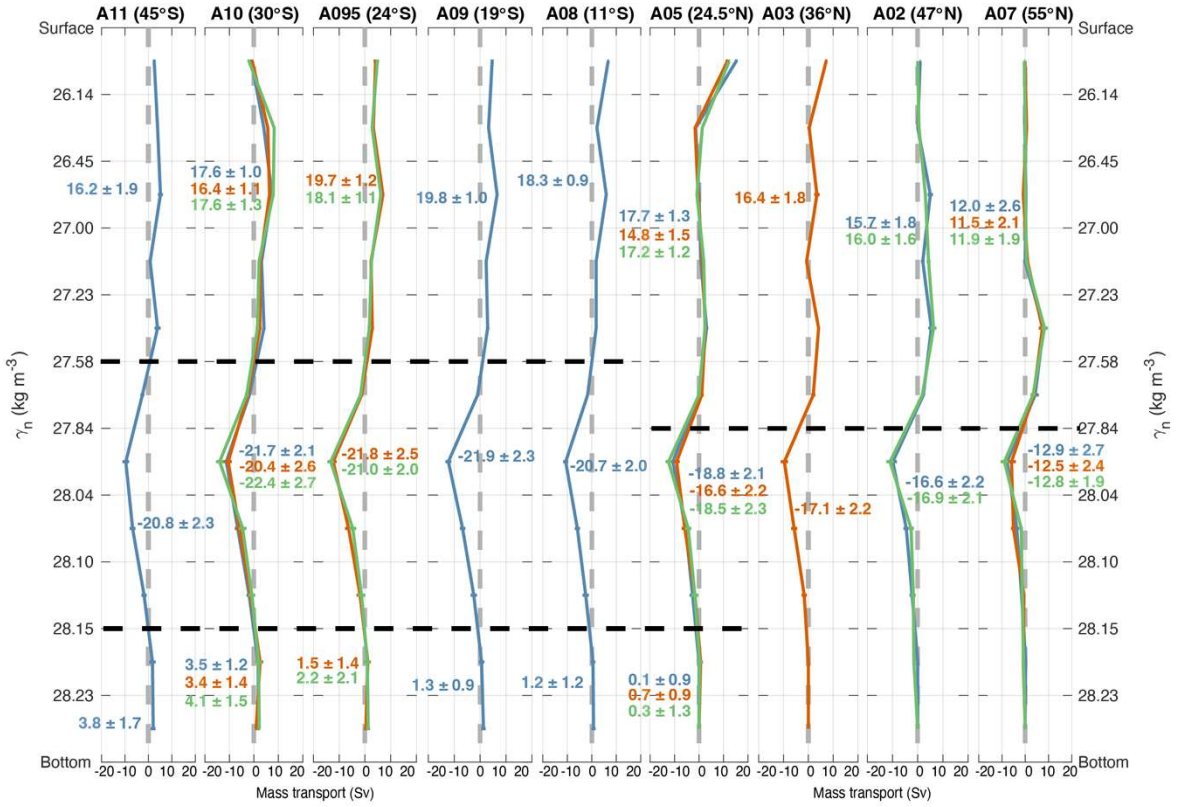

1990-1999 ***2000-2009*** ***2010-2019***

No significant trends for AMOC at any latitude for the last three decades

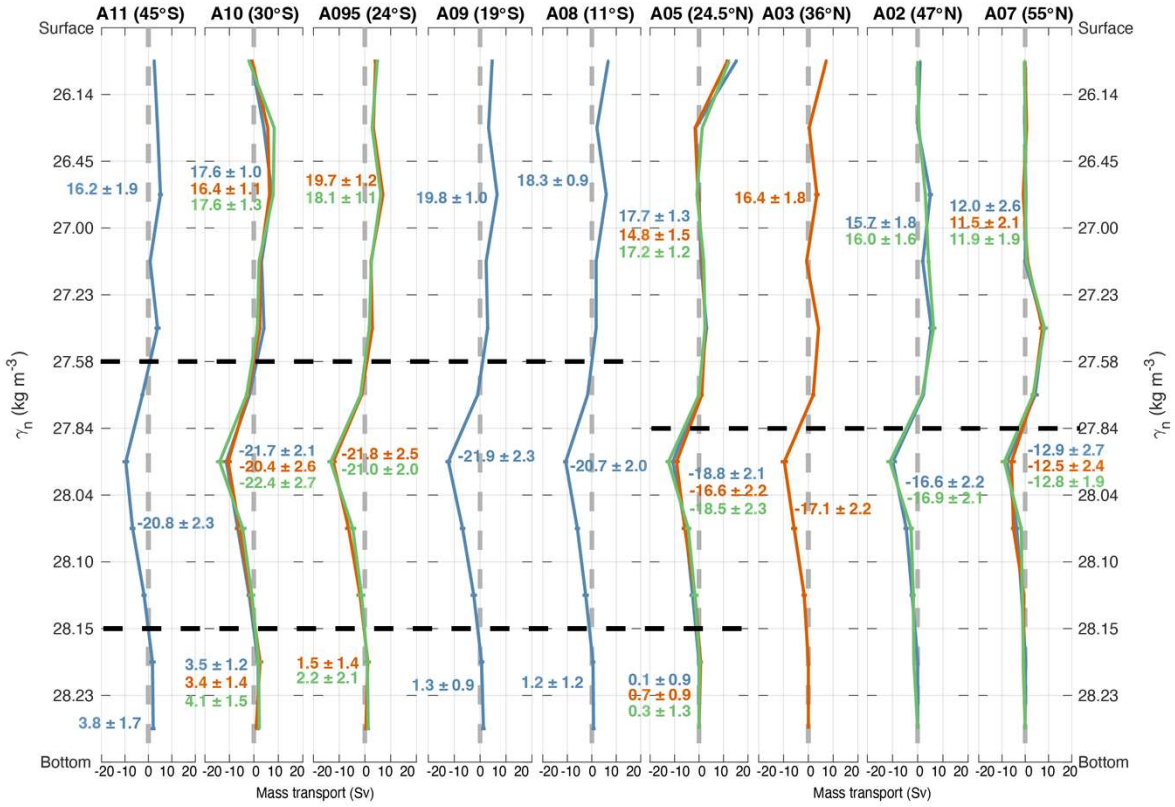

Results for OSNAP line:

Constant weak transport in Labrador Sea
Eastern basin is major contributor to AMOC

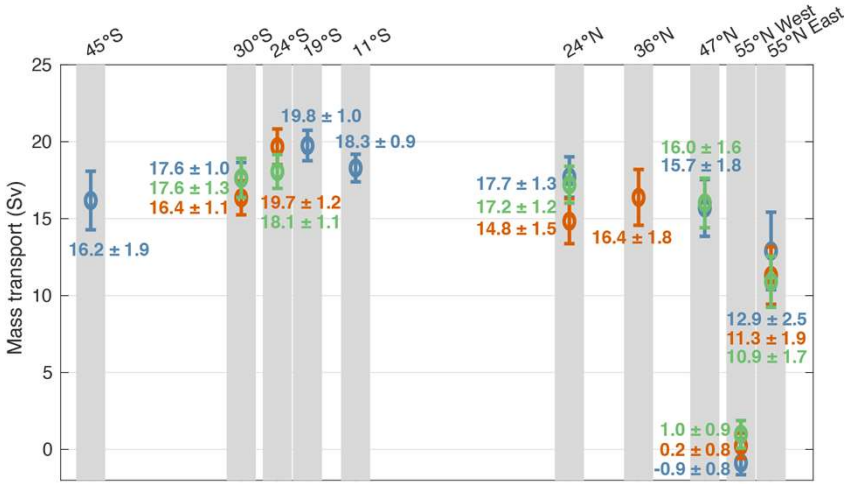

1990-1999 ***2000-2009*** ***2010-2019***

Heat transport by the AMOC

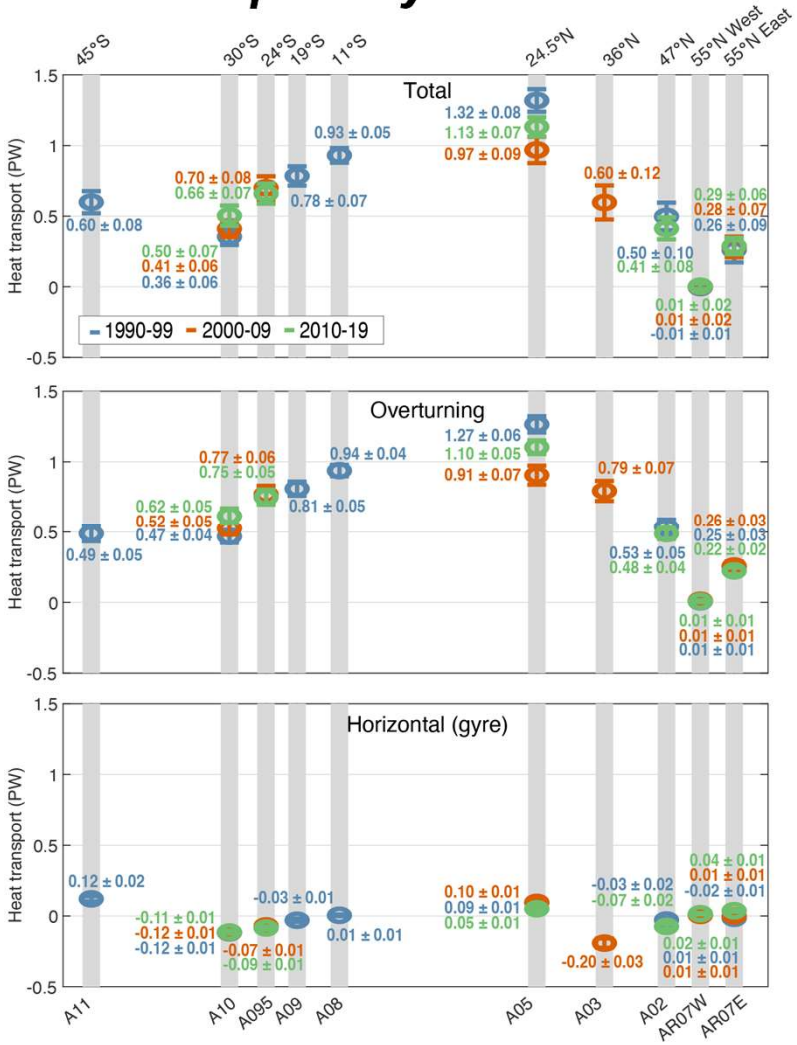

Overturning heat transport, which represents changes in the meridional structure of the water column, dominates the total heat transport and increases equatorward

The horizontal or gyre present constant values across all latitudes and through the decades of this study.

Freshwater transport by the AMOC

The freshwater overturning component presents a stronger southward transport in the sections close to the equator. The south Atlantic subtropical gyre presents low values of overturning freshwater flux at 30°S, with values close to zero at this latitude.

The horizontal or gyre freshwater flux displays a higher northward freshwater flux in the sections that occupy the subtropical gyres, with similar values for all decades.

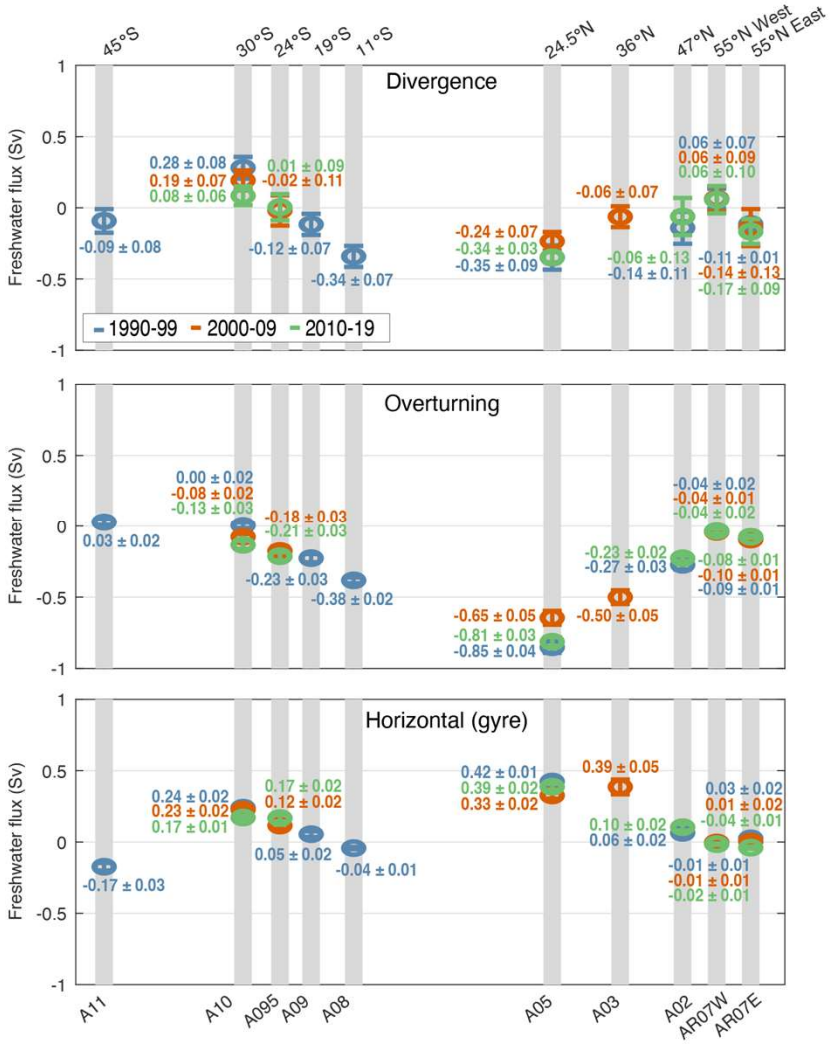

Outline

- Introduction
- AMOC: overturning of mass, heat, freshwater
- **Atlantic budget of Anthropogenic Carbon (C_{anth})**

Caínzos et al., 2022 *(GBC)*

The change of Anthropogenic carbon transport in the ocean

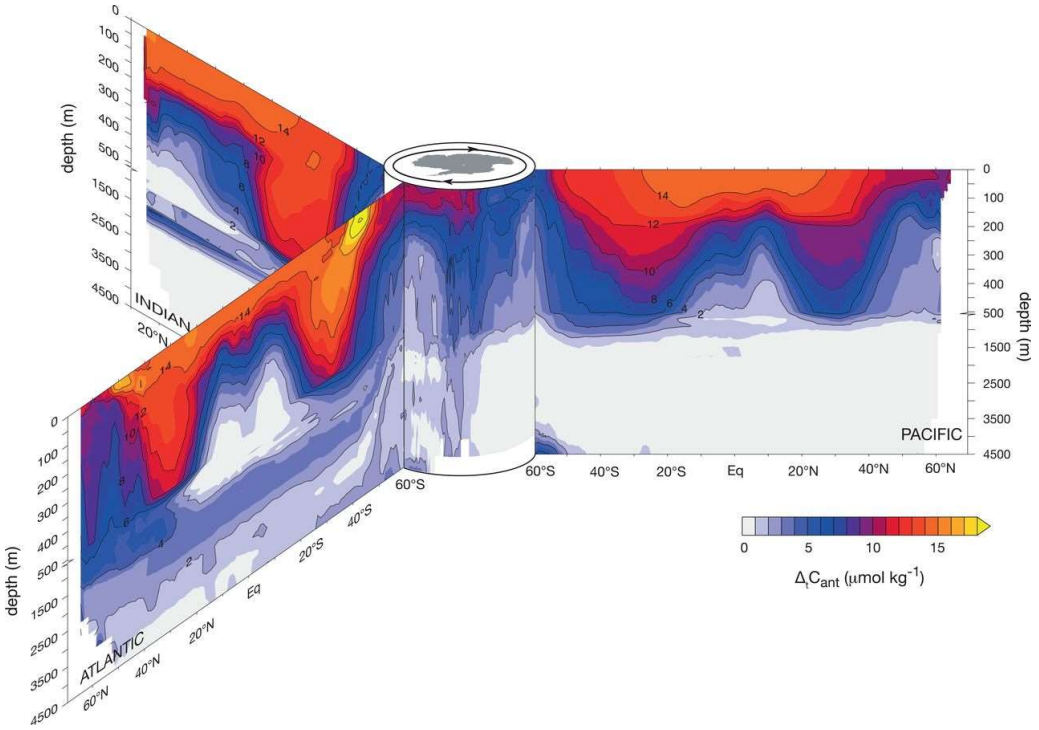

Gruber et al., 2019

The change of Anthropogenic carbon transport in the ocean

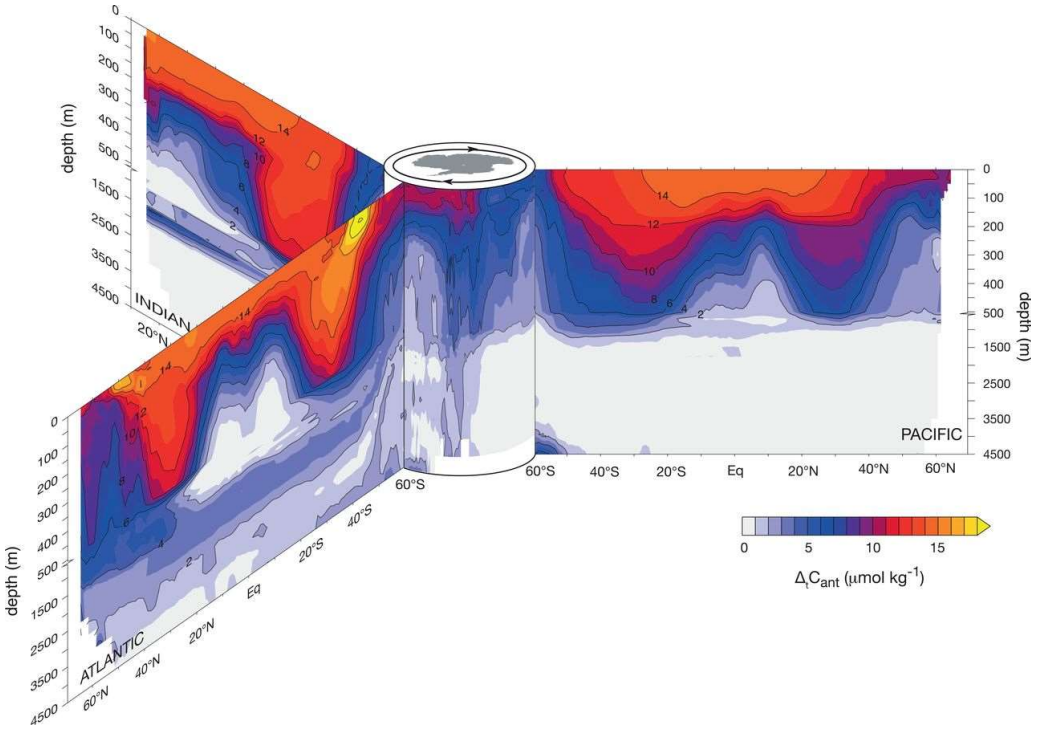

Gruber et al., 2019

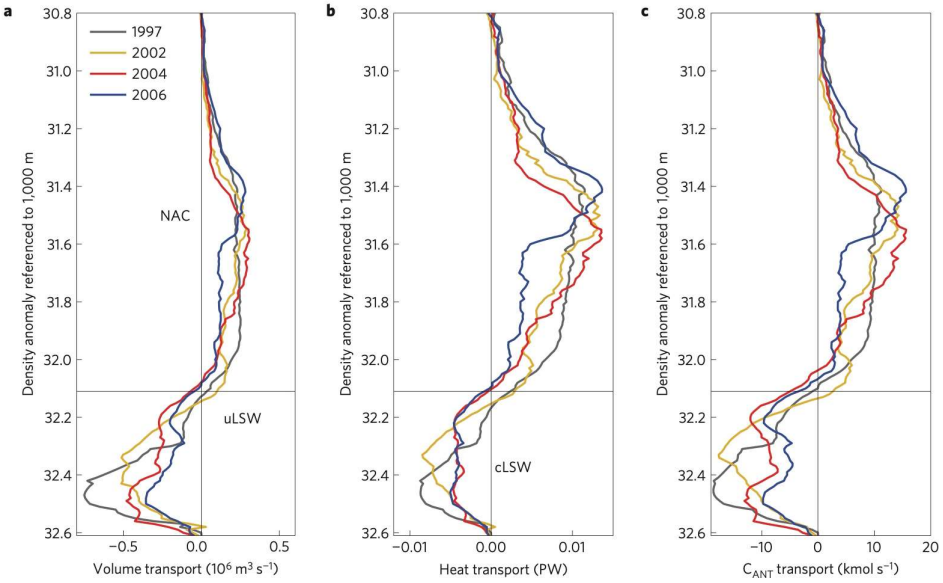

Positive correlation between intensity of AMOC and C_{anth} storage rate in the SPNA

Pérez et al., 2013

Anthropogenic carbon transport with monitoring arrays

RAPID/MOCHA/WBTS

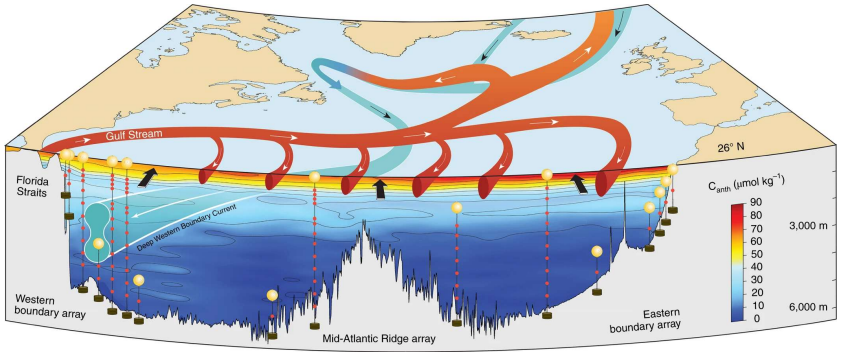

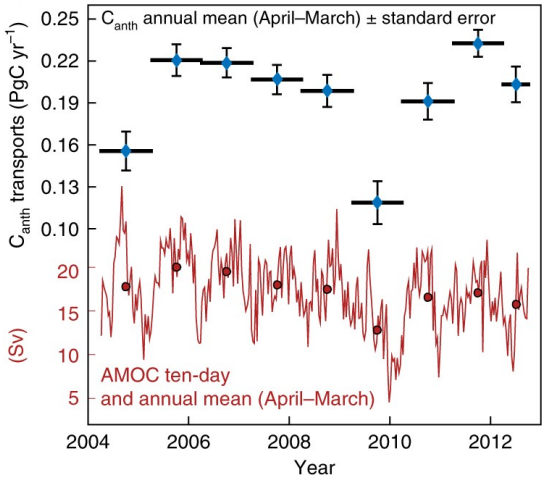

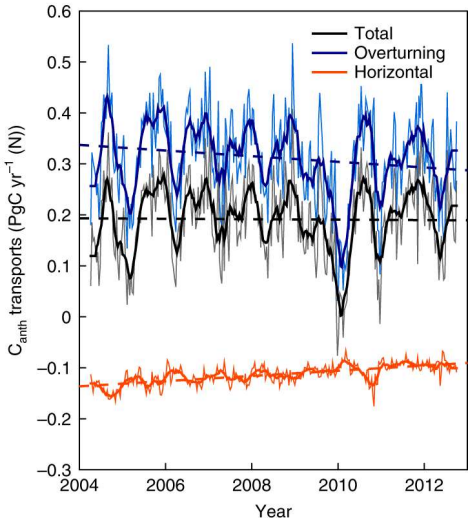

Brown et al., 2021

OVIDE

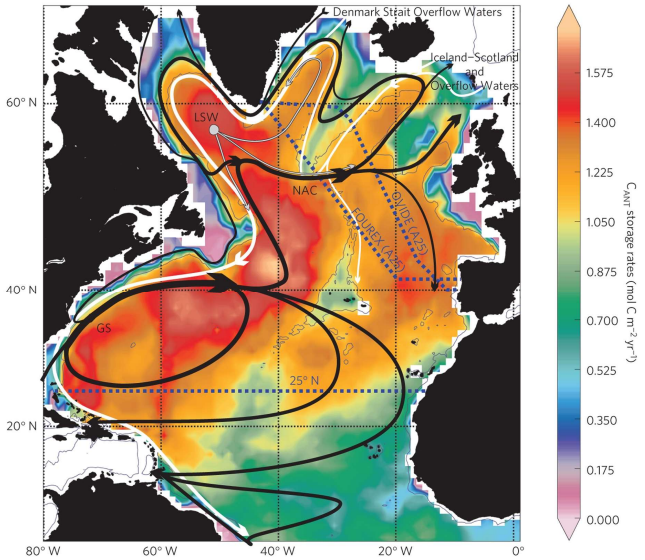

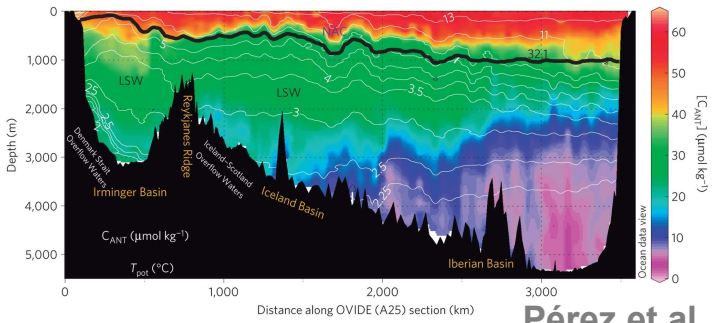

Pérez et al., 2013

Biogeochemical data

Latitude	Section	Year	Code	Dataset
45°S	A11	1992	74DI19921222	GLODAPv2
30°S	A10	1992-93	06MT19921227	GLODAPv2
19°S	A09	1991	06MT19910210	GLODAPv2
11°S	A08	1994	06MT19940329	GLODAPv2
24°N	A05	1992	29HE19920714	GLODAPv2
47°N	A02	1993	06GA19930612	CCHDO
55°N	AR07W	1990	18DA90012	CCHDO
55°N	AR07E	1991	74AB62	CCHDO
30°S	A10	2003	49NZ20031106	GLODAPv2
24°S	A095	2009	740H20090307	GLODAPv2
24°N	A05	2004	74DI20040404	GLODAPv2
36°N	A03	2005	74AB20050501	GLODAPv2
55°N	AR07W	2005	18HU20050526	GLODAPv2
55°N	AR07E	2007	64PE20070830	GLODAPv2
30°S	A10	2011	33RO20110926	GLODAPv2
24°S	A095	2018	740H20180228	GLODAPv2
24°N	A05	2011	29AH20110128	GLODAPv2
47°N	A02	2013	06M220130509	GLODAPv2
55°N	AR07W	2014	74JC20140606	BODC
55°N	AR07E	2014	74JC20140606	BODC

GLODAPv2.2022

Global Ocean Data Analysis Project

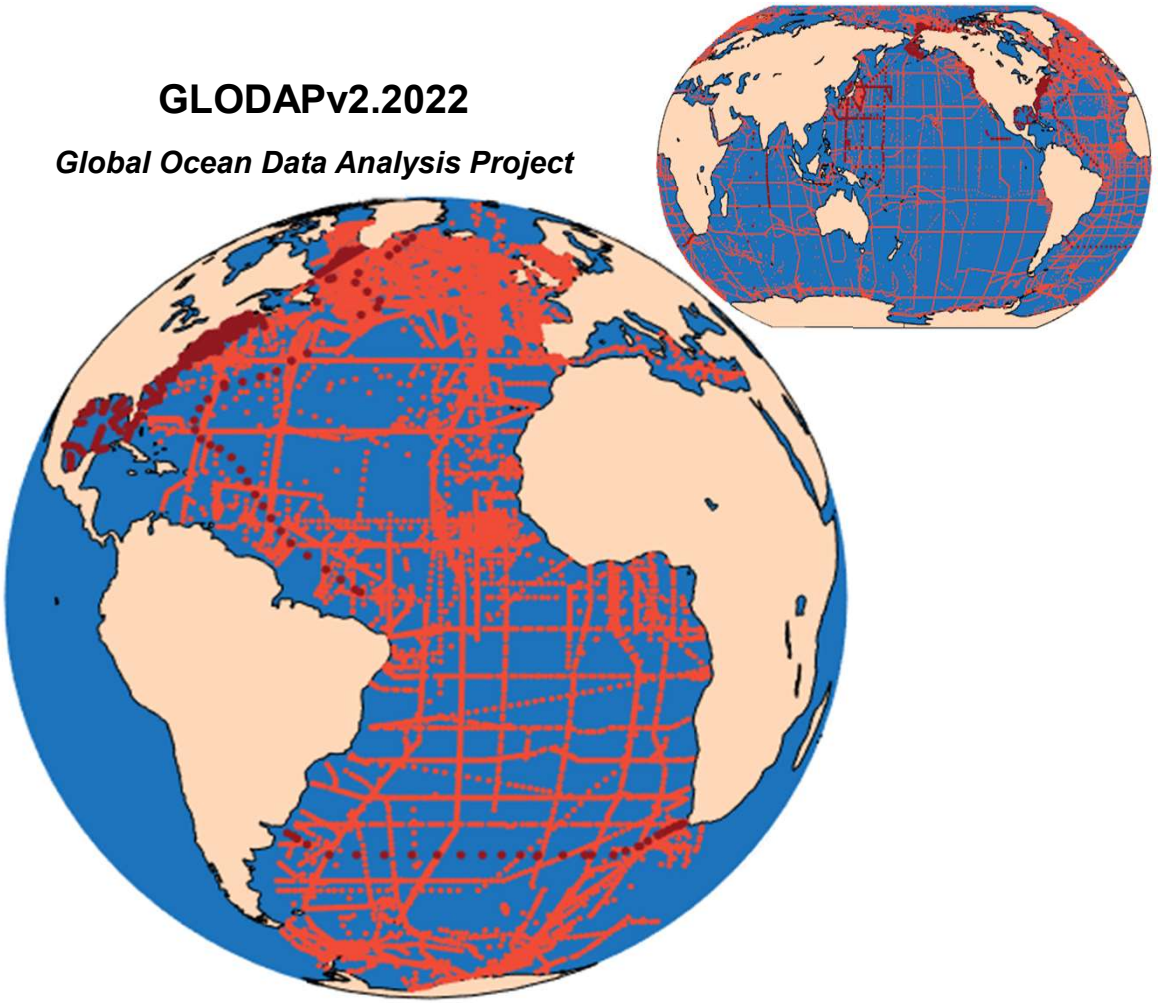

Lauvset et al., 2022

Inverse modelling with biogeochemical variables

$$
\begin{pmatrix}
e_{A_{t,1}} & \cdots & e_{A_{t,n}} & e_{B_{t,1}} & \cdots & e_{B_{t,m}} & 1 & 1 & 0 & 0 & 0 & \cdots & 0 & 0 \\
e_{A_{reg}} & \cdots & e_{A_{reg}} & 0 & \cdots & 0 & 0 & 0 & 0 & 0 & 0 & \cdots & 0 & 0 \\
0 & \cdots & 0 & e_{B_{reg}} & \cdots & e_{B_{reg}} & 0 & 0 & 0 & 0 & 0 & \cdots & 0 & 0 \\
e_{A_{1,1}} & \cdots & e_{A_{1,n}} & e_{B_{1,1}} & \cdots & e_{B_{1,m}} & 1 & 1 & 0 & 0 & 0 & \cdots & 0 & 0 \\
e_{A_{2,1}} & \cdots & e_{A_{2,n}} & e_{B_{2,1}} & \cdots & e_{B_{2,m}} & 0 & 0 & 0 & 0 & 0 & \cdots & 0 & 0 \\
\vdots & \ddots & \vdots & \vdots & \ddots & \vdots & \vdots & \vdots & \vdots & \vdots & \vdots & \ddots & \vdots & \vdots \\
e_{A_{q-1,1}} & \cdots & e_{A_{q-1,n}} & e_{B_{q-1,1}} & \cdots & e_{B_{q-1,m}} & 0 & 0 & 0 & 0 & 0 & \cdots & 0 & 0 \\
e_{A_{q,1}} & \cdots & e_{A_{q,n}} & e_{B_{q,1}} & \cdots & e_{B_{q,m}} & 0 & 0 & 0 & 0 & 0 & \cdots & 0 & 0 \\
s_{A_{t,1}} & \cdots & s_{A_{t,n}} & 0 & \cdots & 0 & \overline{\left(\frac{s_{A_1}}{e_{A_1}}\right)} & 0 & 0 & 0 & 0 & \cdots & 0 & 0 \\
0 & \cdots & 0 & s_{B_{t,1}} & \cdots & s_{B_{t,m}} & 0 & \overline{\left(\frac{s_{B_1}}{e_{B_1}}\right)} & 0 & 0 & 0 & \cdots & 0 & 0 \\
f_{A_{1,1}} & \cdots & f_{A_{1,n}} & f_{B_{1,1}} & \cdots & f_{B_{1,m}} & \overline{\left(\frac{f_{A_1}}{e_{A_1}}\right)} & \overline{\left(\frac{f_{B_1}}{e_{B_1}}\right)} & 1 & 1 & 0 & \cdots & 0 & 0 \\
f_{A_{2,1}} & \cdots & f_{A_{2,n}} & f_{B_{2,1}} & \cdots & f_{B_{2,m}} & 0 & 0 & 0 & 0 & 1 & \cdots & 0 & 0 \\
\vdots & \ddots & \vdots & \vdots & \ddots & \vdots & \vdots & \vdots & \vdots & \vdots & \vdots & \ddots & \vdots & \vdots \\
f_{A_{q-1,1}} & \cdots & f_{A_{q-1,n}} & f_{B_{q-1,1}} & \cdots & f_{B_{q-1,m}} & 0 & 0 & 0 & 0 & 0 & \cdots & 1 & 0 \\
f_{A_{q,1}} & \cdots & f_{A_{q,n}} & f_{B_{q,1}} & \cdots & f_{B_{q,m}} & 0 & 0 & 0 & 0 & 0 & \cdots & 0 & 1 \\
g_{A_{1,1}} & \cdots & g_{A_{1,n}} & g_{B_{1,1}} & \cdots & g_{B_{1,m}} & \overline{\left(\frac{g_{A_1}}{e_{A_1}}\right)} & \overline{\left(\frac{g_{B_1}}{e_{B_1}}\right)} & 0 & r_{NO} & 0 & \cdots & 0 & 0 \\
g_{A_{2,1}} & \cdots & g_{A_{2,n}} & g_{B_{2,1}} & \cdots & g_{B_{2,m}} & 0 & 0 & 0 & 0 & r_{NO} & \cdots & 0 & 0 \\
\vdots & \ddots & \vdots & \vdots & \ddots & \vdots & \vdots & \vdots & \vdots & \vdots & \vdots & \ddots & \vdots & \vdots \\
g_{A_{q-1,1}} & \cdots & g_{A_{q-1,n}} & g_{B_{q-1,1}} & \cdots & g_{B_{q-1,m}} & 0 & 0 & 0 & 0 & 0 & \cdots & r_{NO} & 0 \\
g_{A_{q,1}} & \cdots & g_{A_{q,n}} & g_{B_{q,1}} & \cdots & g_{B_{q,m}} & 0 & 0 & 0 & 0 & 0 & \cdots & 0 & r_{NO} \\
h_{A_{1,1}} & \cdots & h_{A_{1,n}} & h_{B_{1,1}} & \cdots & h_{B_{1,m}} & \overline{\left(\frac{h_{A_1}}{e_{A_1}}\right)} & \overline{\left(\frac{h_{B_1}}{e_{B_1}}\right)} & 0 & r_{SiO} & 0 & \cdots & 0 & 0 \\
h_{A_{2,1}} & \cdots & h_{A_{2,n}} & h_{B_{2,1}} & \cdots & h_{B_{2,m}} & 0 & 0 & 0 & 0 & r_{SiO} & \cdots & 0 & 0 \\
\vdots & \ddots & \vdots & \vdots & \ddots & \vdots & \vdots & \vdots & \vdots & \vdots & \vdots & \ddots & \vdots & \vdots \\
h_{A_{q-1,1}} & \cdots & h_{A_{q-1,n}} & h_{B_{q-1,1}} & \cdots & h_{B_{q-1,m}} & 0 & 0 & 0 & 0 & 0 & \cdots & r_{SiO} & 0 \\
h_{A_{q,1}} & \cdots & h_{A_{q,n}} & h_{B_{q,1}} & \cdots & h_{B_{q,m}} & 0 & 0 & 0 & 0 & 0 & \cdots & 0 & r_{SiO} \\
j_{A_{1,1}} & \cdots & j_{A_{1,n}} & j_{B_{1,1}} & \cdots & j_{B_{1,m}} & \overline{\left(\frac{j_{A_1}}{e_{A_1}}\right)} & \overline{\left(\frac{j_{B_1}}{e_{B_1}}\right)} & 0 & r_{PO} & 0 & \cdots & 0 & 0 \\
j_{A_{2,1}} & \cdots & j_{A_{2,n}} & j_{B_{2,1}} & \cdots & j_{B_{2,m}} & 0 & 0 & 0 & 0 & r_{PO} & \cdots & 0 & 0 \\
\vdots & \ddots & \vdots & \vdots & \ddots & \vdots & \vdots & \vdots & \vdots & \vdots & \vdots & \ddots & \vdots & \vdots \\
j_{A_{q-1,1}} & \cdots & j_{A_{q-1,n}} & j_{B_{q-1,1}} & \cdots & j_{B_{q-1,m}} & 0 & 0 & 0 & 0 & 0 & \cdots & r_{PO} & 0 \\
j_{A_{q,1}} & \cdots & j_{A_{q,n}} & j_{B_{q,1}} & \cdots & j_{B_{q,m}} & 0 & 0 & 0 & 0 & 0 & \cdots & 0 & r_{PO}
\end{pmatrix}
\begin{pmatrix}
b_{A_1} \\ \vdots \\ b_{B_n} \\ b_{B_1} \\ \vdots \\ b_{B_m} \\ \Delta T_{A_{Ek}} \\ \Delta T_{B_{Ek}} \\ \Delta F_{a-s} \\ \Delta B_{O_{21}} \\ \Delta B_{O_{22}} \\ \vdots \\ \Delta B_{O_{2q-1}} \\ \Delta B_{O_{2q}}
\end{pmatrix}
=
\begin{pmatrix}
y_{A_t} + y_{B_t} + T_{A_{Ek}} + T_{B_{Ek}} \\
y_{A_{reg}} \\
y_{B_{reg}} \\
y_{A_1} + y_{B_1} + T_{A_{Ek}} + T_{B_{Ek}} \\
y_{A_2} + y_{B_2} \\
\vdots \\
y_{A_{q-1}} + y_{B_{q-1}} \\
y_{A_q} + y_{B_q} \\
z_{A_t} + T_{A_{Ek}} \overline{\left(\frac{S_{A_1}}{e_{A_1}}\right)} \\
z_{B_t} + T_{B_{Ek}} \overline{\left(\frac{S_{B_1}}{e_{B_1}}\right)} \\
k_{A_1} + k_{B_1} + T_{A_{Ek}} \overline{\left(\frac{f_{A_1}}{e_{A_1}}\right)} + T_{B_{Ek}} \overline{\left(\frac{f_{B_1}}{e_{B_1}}\right)} + F_{a-s} + B_{O_{21}} \\
k_{A_2} + k_{B_2} + B_{O_{22}} \\
\vdots \\
k_{A_{q-1}} + k_{B_{q-1}} + B_{O_{2q-1}} \\
k_{A_q} + k_{B_q} + B_{O_{2q}} \\
r_{A_1} + r_{B_1} + T_{A_{Ek}} \overline{\left(\frac{g_{A_1}}{e_{A_1}}\right)} + T_{B_{Ek}} \overline{\left(\frac{g_{B_1}}{e_{B_1}}\right)} + B_{O_{21}} \cdot r_{NO} \\
r_{A_2} + r_{B_2} + B_{O_{22}} \cdot r_{NO} \\
\vdots \\
r_{A_{q-1}} + r_{B_{q-1}} + B_{O_{2q-1}} \cdot r_{NO} \\
r_{A_q} + r_{B_q} + B_{O_{2q}} \cdot r_{NO} \\
t_{A_1} + t_{B_1} + T_{A_{Ek}} \overline{\left(\frac{h_{A_1}}{e_{A_1}}\right)} + T_{B_{Ek}} \overline{\left(\frac{h_{B_1}}{e_{B_1}}\right)} + B_{O_{21}} \cdot r_{SiO} \\
t_{A_2} + t_{B_2} + B_{O_{22}} \cdot r_{SiO} \\
\vdots \\
t_{A_{q-1}} + t_{B_{q-1}} + B_{O_{2q-1}} \cdot r_{SiO} \\
t_{A_q} + t_{B_q} + B_{O_{2q}} \cdot r_{SiO} \\
u_{A_1} + u_{B_1} + T_{A_{Ek}} \overline{\left(\frac{j_{A_1}}{e_{A_1}}\right)} + T_{B_{Ek}} \overline{\left(\frac{j_{B_1}}{e_{B_1}}\right)} + B_{O_{21}} \cdot r_{PO} \\
u_{A_2} + u_{B_2} + B_{O_{22}} \cdot r_{PO} \\
\vdots \\
u_{A_{q-1}} + u_{B_{q-1}} + B_{O_{2q-1}} \cdot r_{PO} \\
u_{A_q} + u_{B_q} + B_{O_{2q}} \cdot r_{PO}
\end{pmatrix}
$$

e: mass
s: salt
f: oxygen
g: nitrate
h: silicate
j: phosphate

y: mass transport
z: salt transport
k: oxygen transport
r: nitrate transport
t: silicate transport
u: phosphate transport

b: reference velocities
T_{Ek}: Ekman transport
ΔT_{Ek}: Ekman correction
$F_{a\text{-}s}$: oxygen influx from the air- sea interphase
$\Delta F_{a\text{-}s}$: adjustment of oxygen influx
B_{O2}: sources and sinks of oxygen in water column
ΔB_{O2}: adjustment of oxygen consumption
r_{NO}: Redfield ratio N-O
r_{SiO}: Redfield ratio Si-O
r_{PO}: Redfield ratio P-O

n: number of pair of stations for section A
m: number of pair of stations for section B
q: number of layers (11)

C_{anth} transport divided into components

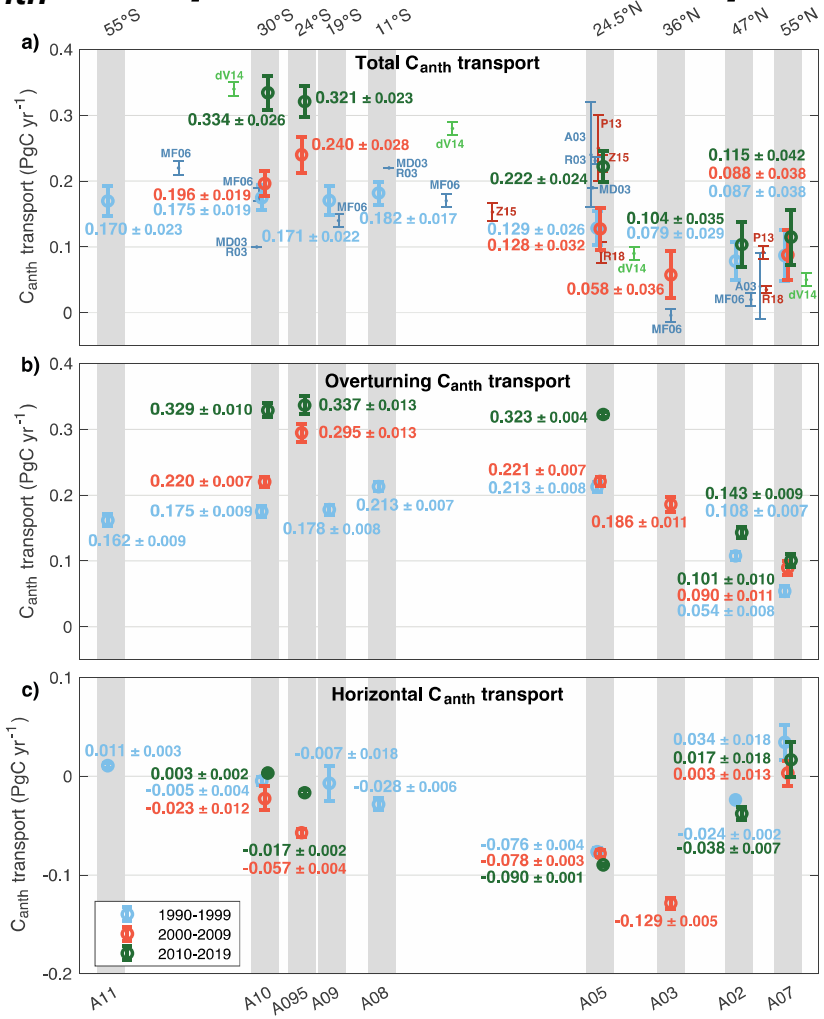

C_{anth} transport divided into components

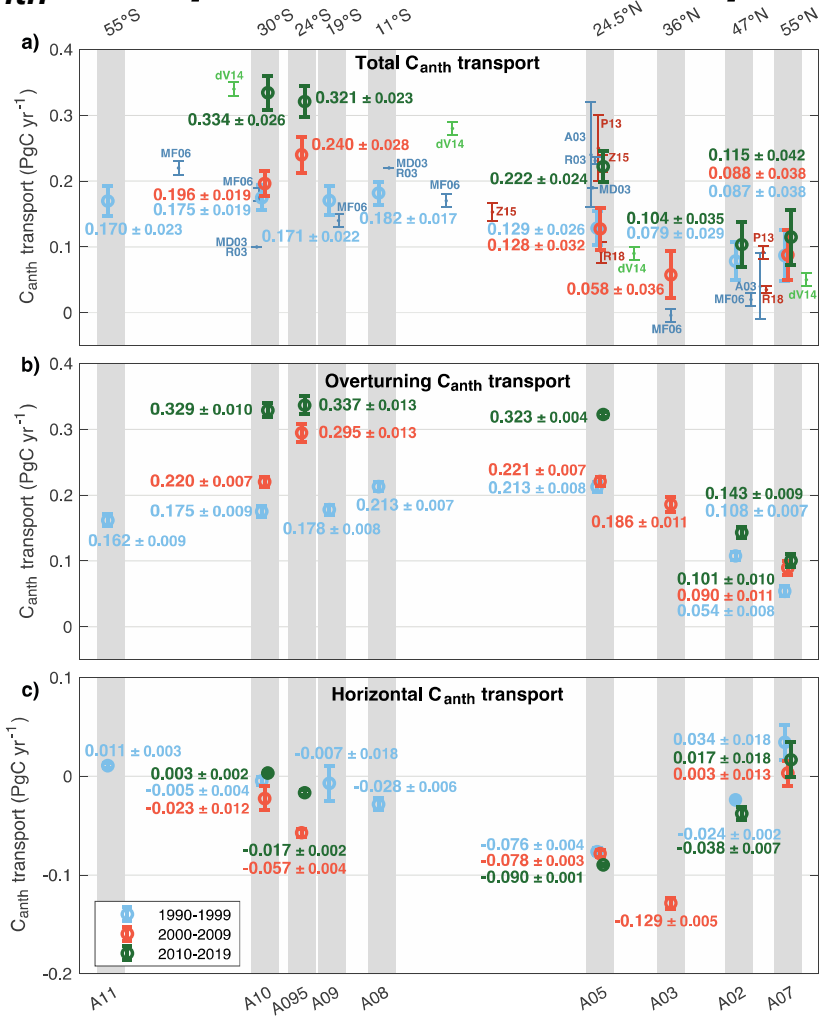

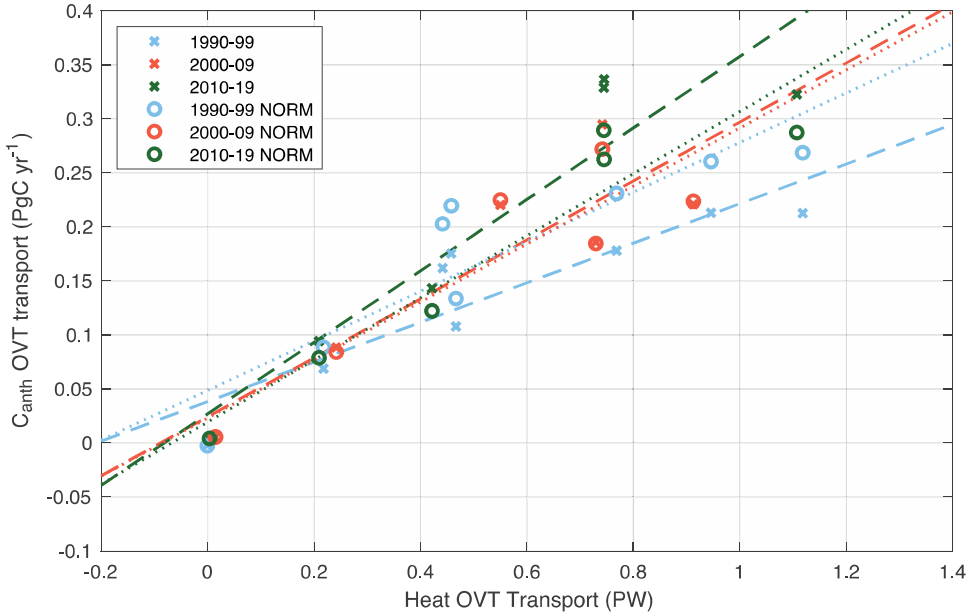

Atlantic C_{anth} transport **Results & Discussion**

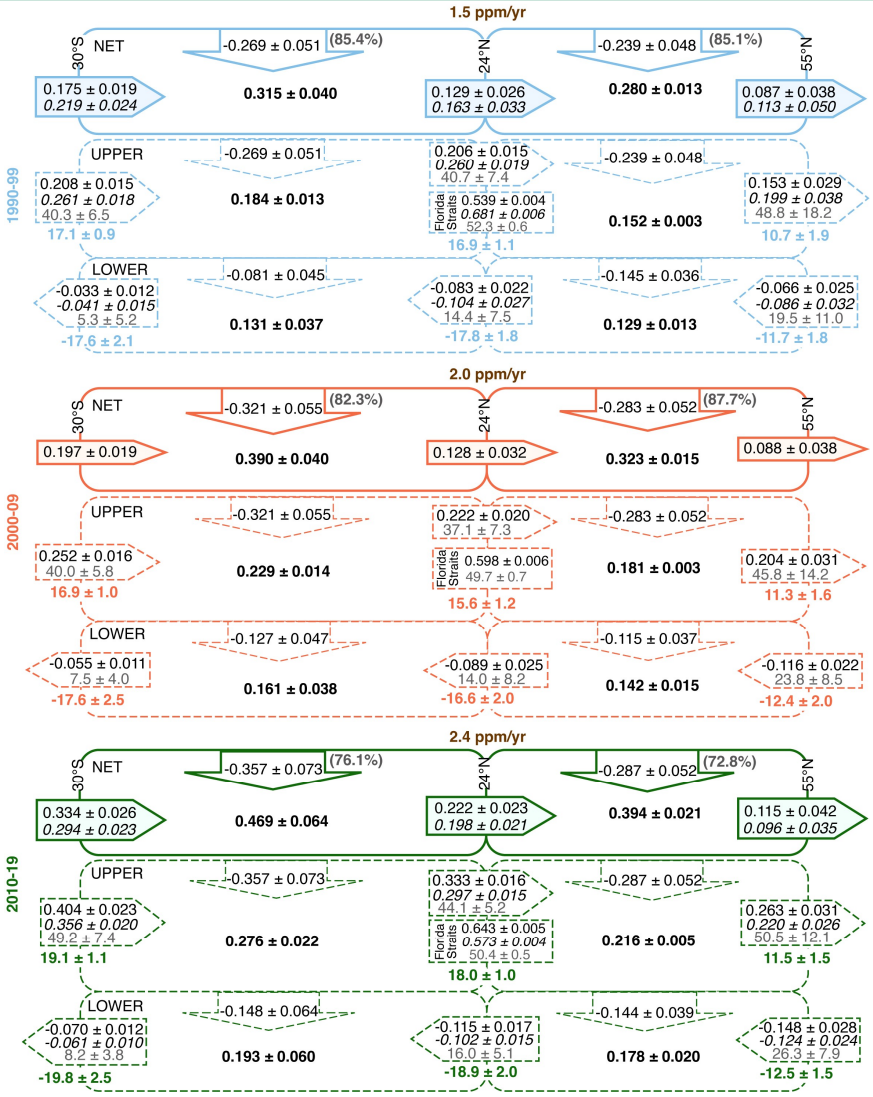

C_{anth} transport and storage budgets

Decreasing northward transport from recent central and intermediate waters from Southern Ocean

Atlantic C_{anth} transport **Results & Discussion**

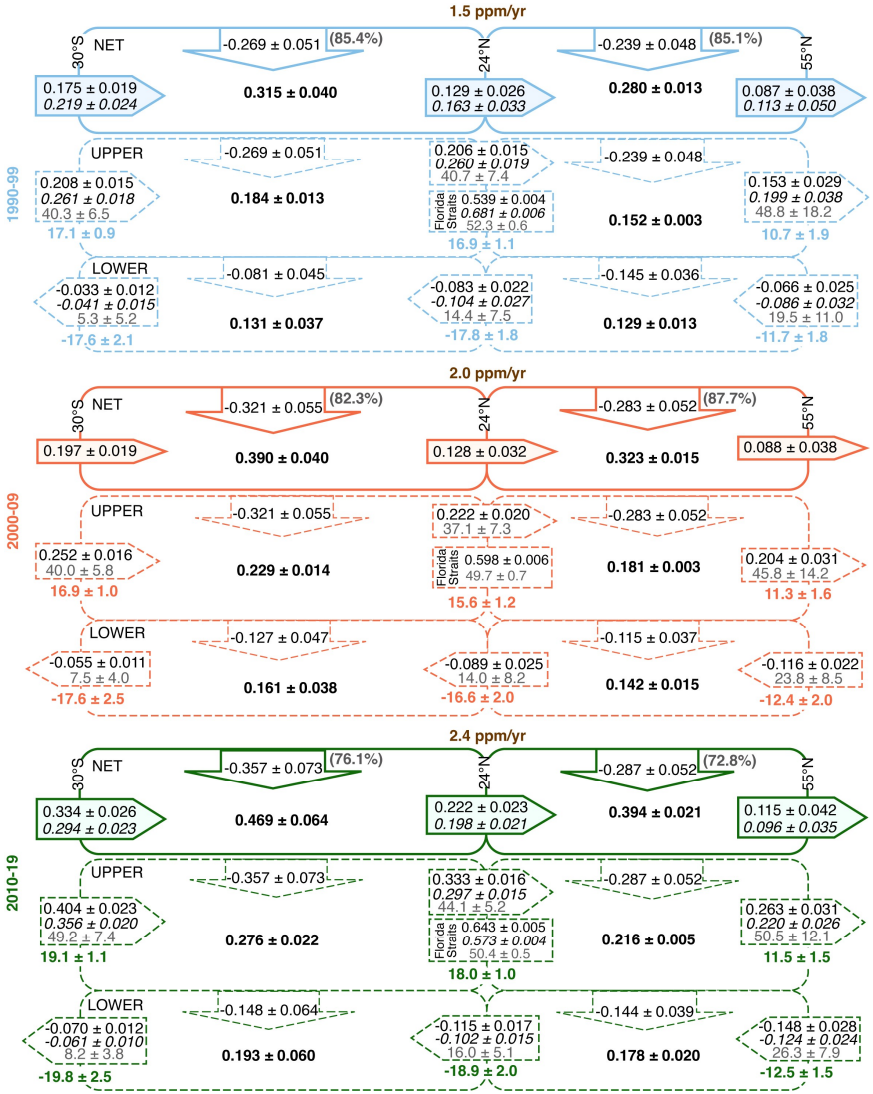

C_{anth} transport and storage budgets

Decreasing northward transport from recent central and intermediate waters from Southern Ocean

Transports at 24ºN show weaker values for 2000-09, with recuperation for last decade

Atlantic C_{anth} transport Results & Discussion

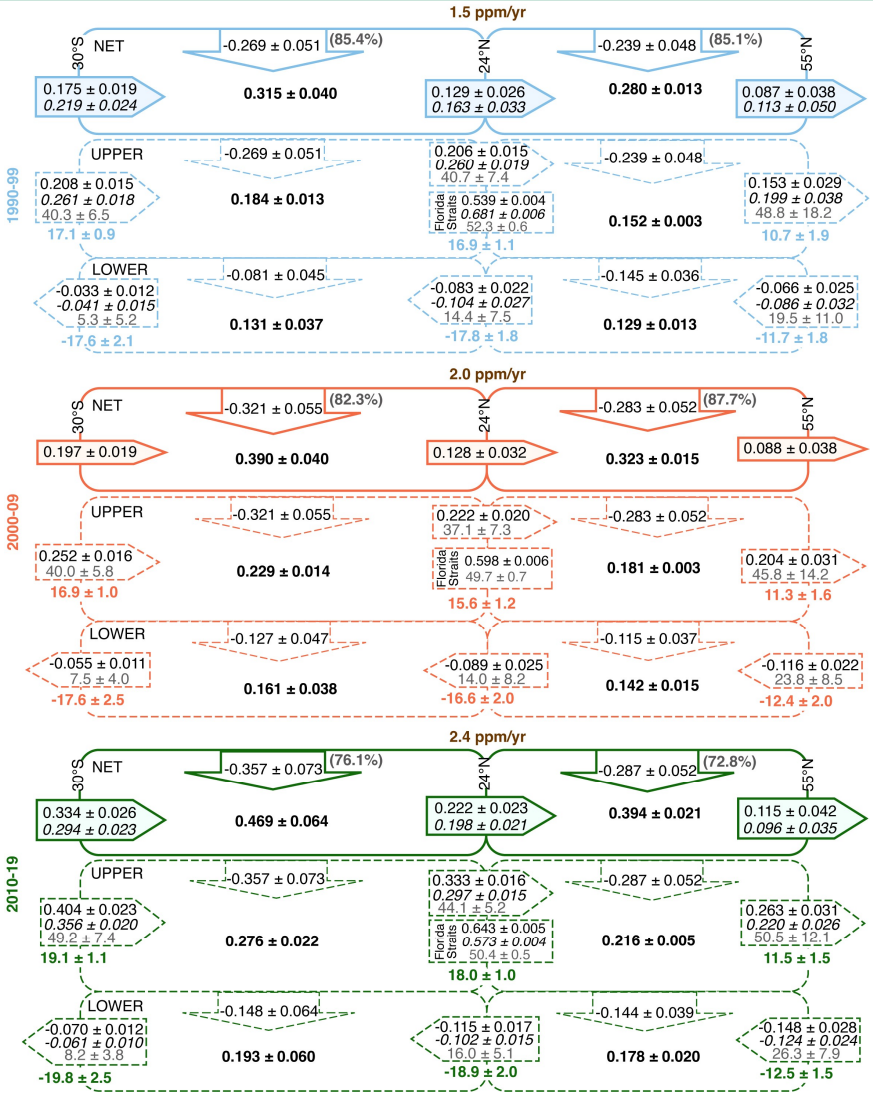

C_{anth} transport and storage budgets

Decreasing northward transport from recent central and intermediate waters from Southern Ocean

Transports at 24ºN show weaker values for 2000-09, with recuperation for last decade

Strong lateral transports at 55ºN with deep convection carrying C_{anth} into Nordic Seas

Vertical transport of C_{anth} transport

Overturning in North Atlantic redistributes the newly gained C_{anth} from the atmosphere, exporting to deep layers

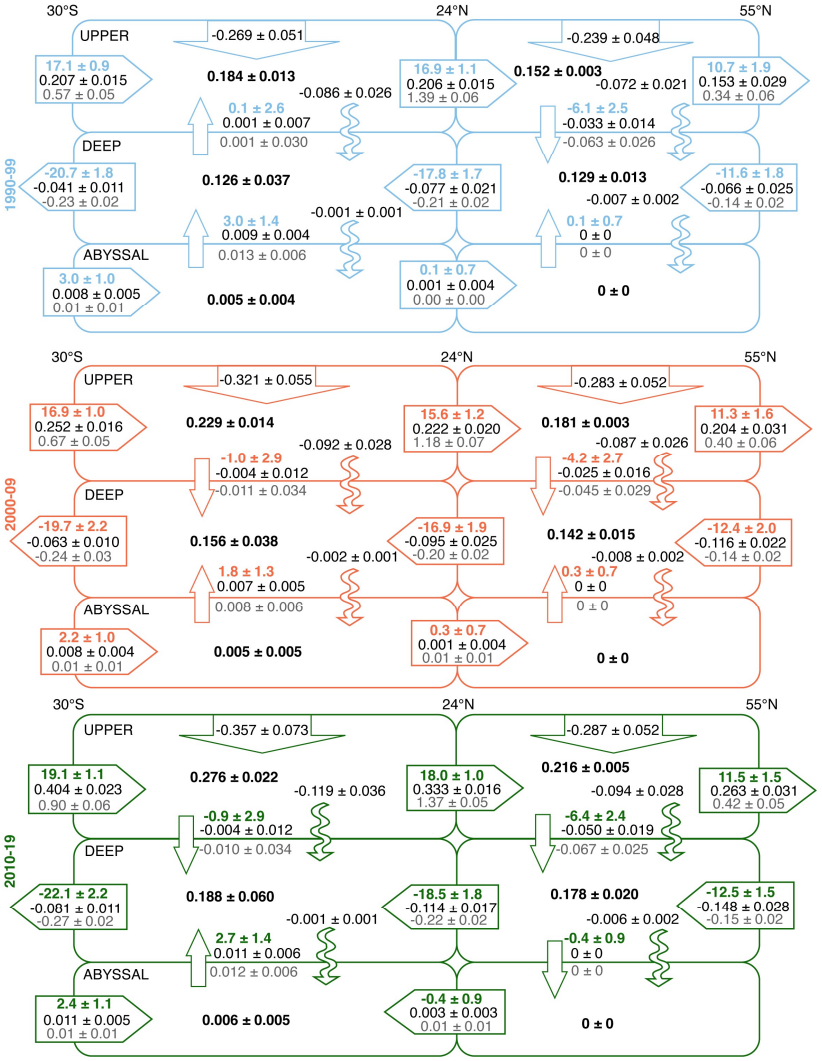

Vertical transport of C_{anth} transport

Overturning in North Atlantic redistributes the newly gained C_{anth} from the atmosphere, exporting to deep layers

Abyssal layers in South Atlantic introduce C_{anth} from AABW with an upward flux to deep layers

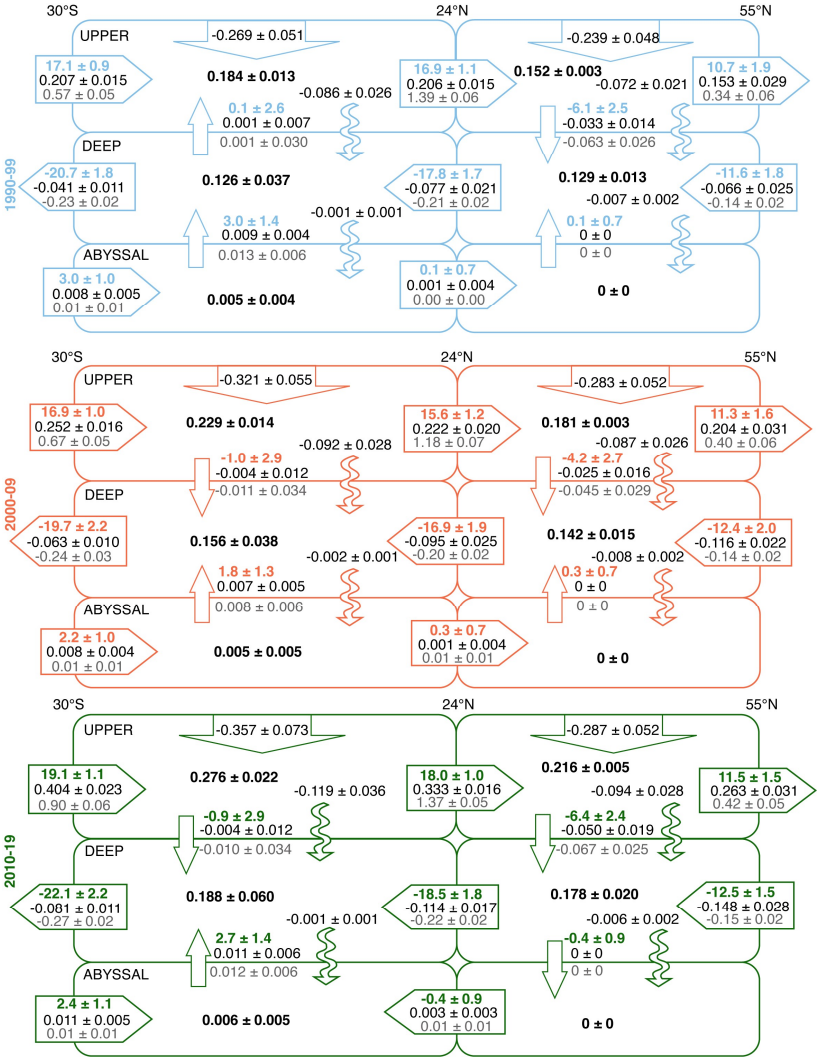

Vertical transport of C_{anth} transport

Overturning in North Atlantic redistributes the newly gained C_{anth} from the atmosphere, exporting to deep layers

Abyssal layers in South Atlantic introduce C_{anth} from AABW with an upward flux to deep layers

Mixing by diffusion occurs in the whole basin mainly between upper and deep layers

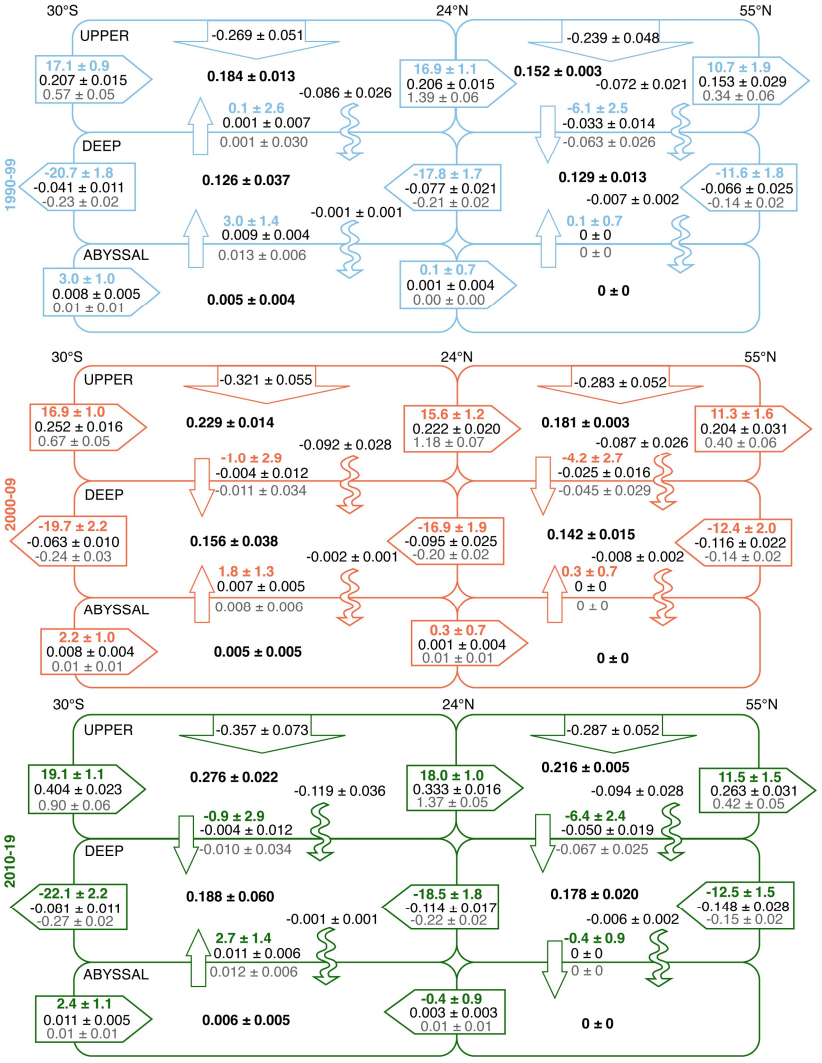


Thanks for your attention!

Aliasing Inverse model: single vs multiple sections

Caínzos et al., 2023 (*GRL*)

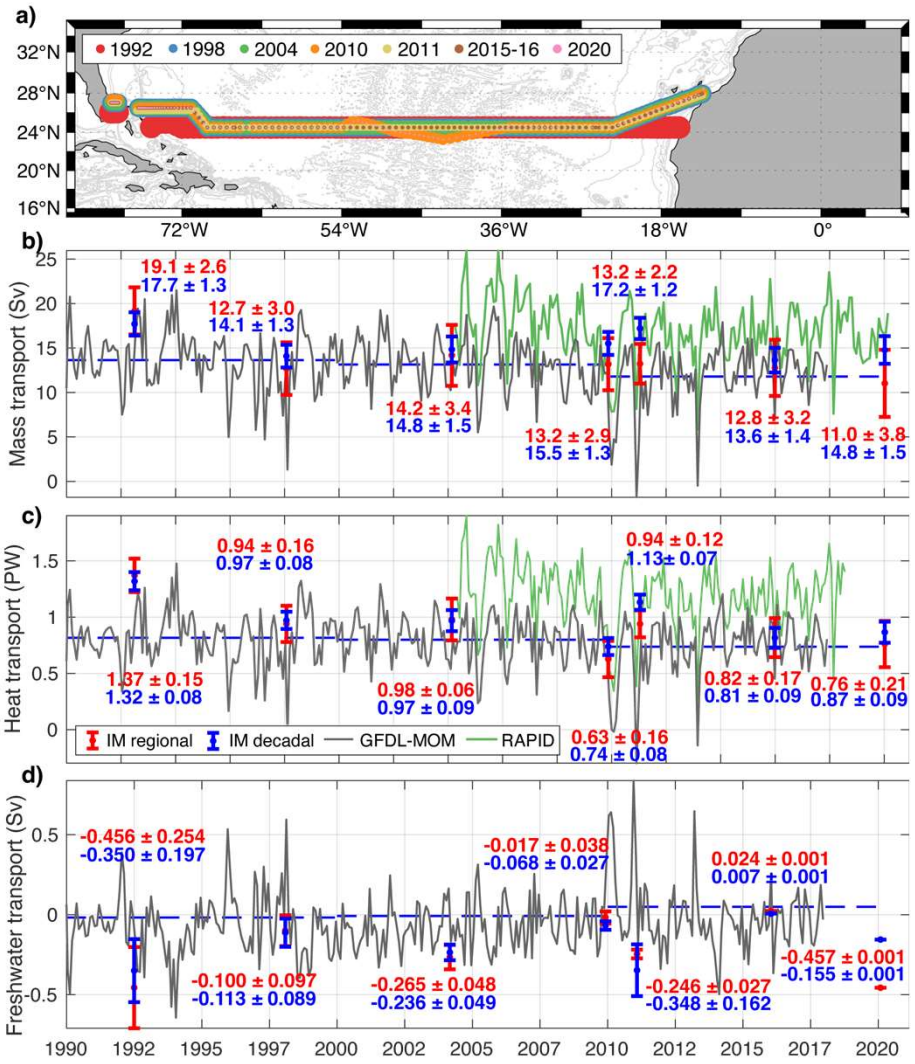

Comparison for 24.5°N

		GFDL-MOM cruise	GFDL-MOM decadal
Single-section inverse model	RMSE AMOC (Sv)	**1.8**	2.4
	RMSE MHT (PW)	**0.18**	0.19
	RMSE MFT (Sv)	**0.220**	0.280
Multiple-section inverse model	RMSE AMOC (Sv)	3.9	**1.5**
	RMSE MHT (PW)	0.19	**0.15**
	RMSE MFT (Sv)	0.277	**0.267**

Inverse solutions from single sections are affected by aliasing, as they capture the circulation structure of the time of the cruise.

Inverse models with multiple sections at different latitudes and times agree with decadal averages from an ocean general circulation model.

Aliasing Inverse model: single vs multiple sections

Caínzos et al., 2023 (*GRL*)

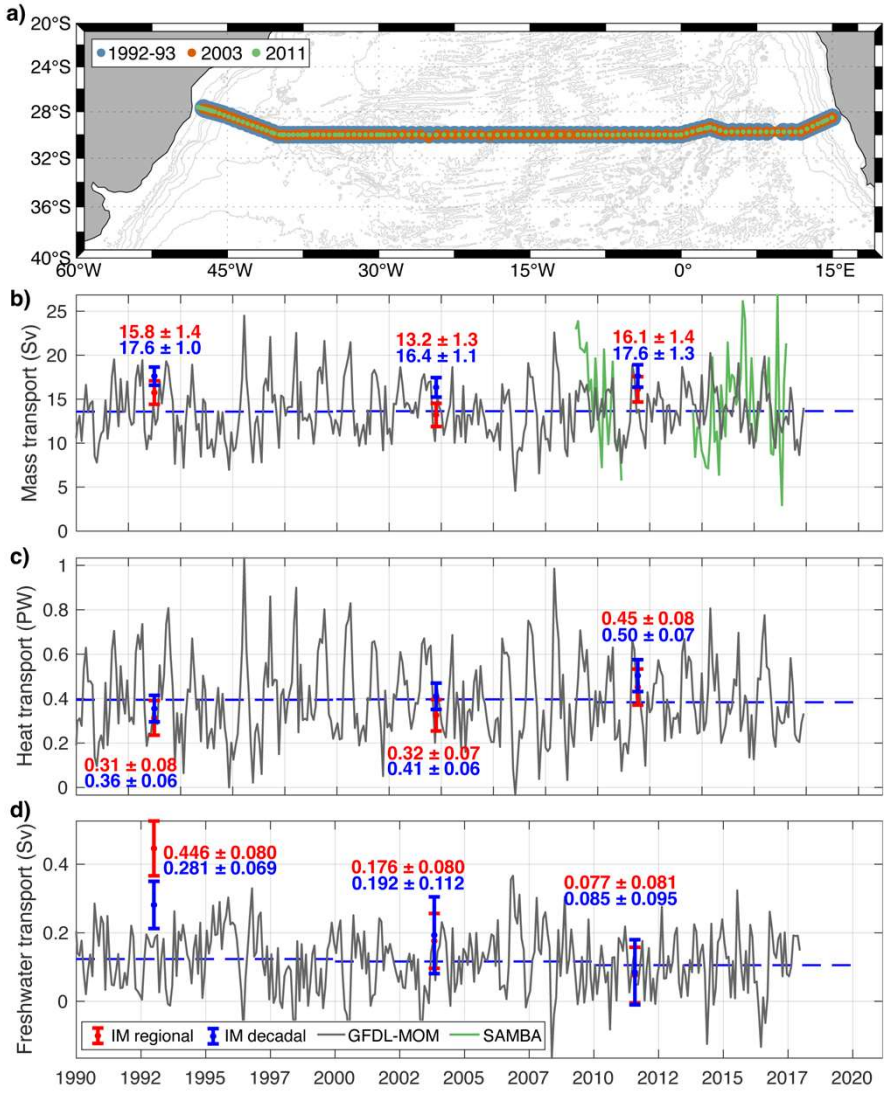

Comparison for 30°S

		GFDL-MOM cruise	GFDL-MOM decadal
Single-section inverse model	RMSE AMOC (Sv)	**0.9**	1.4
	RMSE MHT (PW)	**0.05**	0.07
	RMSE MFT (Sv)	**0.180**	0.193
Multiple-section inverse model	RMSE AMOC (Sv)	2.9	**2.6**
	RMSE MHT (PW)	0.09	**0.07**
	RMSE MFT (Sv)	**0.084**	0.104

Inverse solutions from single sections are affected by aliasing, as they capture the circulation structure of the time of the cruise.

Inverse models with multiple sections at different latitudes and times agree with decadal averages from an ocean general circulation model.